Performance of CIMMINO and Pencil Beam Convolution Photon Dose Calculation Algorithm in Lung Intensity Modulated Radiation Therapy

By:

Talat Mahmood
(04-FBAS/MSPHY/F10)

Supervised by:

Professor Dr. Muhammad Afzal Khan
DEPARTMENT OF PHYSICS
THE ISLAMIA UNIVERSITY OF BAHAWALPUR, PAKISTAN
(2012)

Co-Supervisor:

Dr. Waqar Adil Syed
Associate Professor / Chairman

DEPARTMENT OF PHYSICS
Faculty of Basic and Applied Sciences
INTERNATIONAL ISLAMIC UNIVERSITY OF ISLAMABAD, PAKISTAN
(2012)

Pencil Beam Algorithms

International Islamic University Islamabad
Faculty of Basic & Applied Sciences
Department of Physics

2012

"Performance of CIMMINO and Pencil Beam Convolution Photon Dose Calculation Algorithm in Lung Intensity Modulated Radiation Therapy"

By

Talat Mahmood
(04-FBAS/MSPHY/F10)

This thesis is submitted to Department of Physics, FBAS International Islamic University Islamabad for award of Master of Science Physics Degree (MS Physics).

Chairman, Department of Physics

CHAIRMAN
DEPT. OF PHYSICS
International Islamic University
Islamabad

Act. Dean, FBAS, IIU, Islamabad

DEAN
Faculty of Basic & Applied Sciences
International Islamic University
Islamabad

International Islamic University, Islamabad
Faculty of Basic and Applied Sciences
Department of Physics

Dated: May, 2012

Final Approvai

It is certified that the work presented in this thesis entitled "Performance of CIMMINO and Pencil Beam Convolution Photon Dose Calculation Algorithm in Lung Intensity Modulated Radiation Therapy" by **TalatMahmood, Registration No. 04-FBAS/MSPHY/F10** is of sufficient standard in scope and quality for the award of degree of MS Physics from International Islamic University, Islamabad.

Committee

External Examiner
Dr.Muhammad Ikram Shahzad
Deputy Chief Scientist, PINSITCH
Islamabad, Pakistan

Internal Examiner
Dr. Zafar Wazir
Assistant Professor.
Department of Physics
International Islamic University, Islamabad, Pakistan

Supervisor
Professor Dr.Muhammad Afzal Khan
Department of Physics
The Islamia University of Bahawalpure, Pakistan

Co-Supervisor
Dr. Waqar Adil Syed
Associate Professor,
Chairman, Department of Physics
International Islamic University, Islamabad, Pakistan

Declaration

I hereby declare that this thesis work, neither as a whole nor a part of it has been copied out from any source. Further, work presented in this dissertation has not been submitted in support of any application for any other degree or qualification to any other university or institute. If any part of this project is proved to be copied from any source or found to be reproduction of some other project, I shall be legally responsible for punishment under the plagiarism rules of Higher Education Commission (HEC), Pakistan.

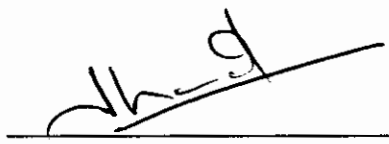

Name: Talat Mahmood
Registration Number: (04-FBAS/MSPHY/F10)

DEDICATION

TO

My Loving Wife, Daughters,

Lovely Parents,

Brothers and Sister

Whose gratis love,

And continuous encouragement

Enable me to score this glory of my life.

Acknowledgements

Up and above anything else, all praises are due to Almighty Allah alone. The omnipotent, the omnipresent, the most merciful and the most compassionate, who blessed me with sound health, sympathetic teachers and friends .I express my deepest gratitude to Almighty Allah for enabling me to complete this research work. I also offer my humblest thanks to Holy Prophet (PBHU) whose teachings are always a source of guidance and beacon for humanity at large.

I deem it a rare privilege and a source of pleasure in expressing my profound and cordial gratitude to my respected, earnest and severed research supervisor, "Professor Dr. Muhammad Afzal Khan" (Department of Physics, The Islamia University of Bahawalpur, Pakistan). Their clear remarks, sense of great vision, salient attitude, and valuable advises and discussions were always a source of candle for me.

I am just unable to find suitable words to pay tribute to my Co- supervisor Dr. Waqar Adil Syed" (Chairman of Physics Department, International Islamic University Islamabad, Pakistan) for his painstaking efforts; keen interest, valuable suggestions, skilled advises, inspiring, Strict and positive criticism in accomplishing this work. It was his motivation and cooperation that I am able to complete this work.

It is a debt of honor for me to express my deep sense of gratitude to my respected professional coworkers Mr. Haseeb Ullah (Medical Physicist, Shifa International Hospital Limited Islamabad, Pakistan), Mr. Muhammad Usman and Muhammad Aqeel Hussain (Medical Physicist, Shaukat Khanum Memorial Cancer Hospital and Research Centre Lahore, Pakistan) who always encouraged me to accomplish this difficult task and give valuable advices and keen interest with sense of great vision and attitude. I am also really thankful to Muhammad Abdul Rafay Chief Medical Physicist of Shaukat Khanum Memorial Cancer Hospital and Research Centre Lahore, Pakistan for cooperation which able me to complete this research work.

I would like to thank my friend Mr. Asif Shehzad Ahmed for his cooperation and valuable efforts. No acknowledgement would ever adequately express my obligation to my parents and wife Kalsoom Rasheed who have always wished to see me flying high above the skies of success. Without their prayers, sacrifice, encouragement, moral support, the present research work would have been a merry dream.

Talat Mahmood

Table of Contents

List of Figures

List of Table

List of Abbreviations

AAPM	American Association of Physicist in Medicine
BEV	Beam Eye View
CPE	Charged Particle Equilibrium
CSDA	Continuous Slowing Down Approximation
CT	Computer Tomography
Dmin.	Minimum Dose
Dmax.	Maximum Dose
Dmean	Mean Dose
DVH	Dose Volume Histograms
FWHM	Full Width At Half Maximum
GTV	Gross Tumor Volume
HI	Homogeneity Index
ICF	Inhomogeneity Correction Factor
ICRU	International Commission of Radiology Units
IMRT	Intensity Modulated Radiotherapy
KERMA	Kinetic Energy Released Per Unit Mass
MC	Manti Carlo
MLC's	Multileaf Collimators
MU	Monitor Unit
MV	Mega Voltage
NSCLC	Non-Small-Cell Lung Cancer
NTCP	Normal Tissue Complication Probability
OARs	Origins at Risks
PB	Pencil Beam
PBC	Pencil Beam Convolution
PDD	Percentage Depth Dose
P-Lung	Normal Lungs
PTV	Planning Tumor Volume
QA	Quality Assurance
SAR	Scatter Air Ratio

SIH	Shifa International Hospital
TAR	Tissue Air Ratio
TCPE	Transient Charged Particle Equilibrium
TG	Task Group
TPR	Tissue Phantom Ratio
TPS	Treatment Planning System
TERMA	Total Energy Released per Unit Mass

ABSTRACT

A comparative study was carried out between Pencil Beam Convolution (PBC) and CIMMINO photon dose calculation algorithms in lung Intensity Modulated Radiation Therapy (IMRT). In this study five non-small cell lung cancer (NSCLC) patients were selected, with differences location tumour. IMRT treatment plans was generated and optimized with the PBC and CIMMINO Algorithms. Investigation of these two external beam dose calculation algorithms based on percentage Isodose distribution, hotspot, dose volume histograms (DVH) and minimum, maximum, mean dose in organs at risk (OARs). Similar procedure was adopted for planning target volume (PTV). The evaluation parameter for PTV is incorporated by homogeneity index (HI). CIMMINO algorithm showed better results than the PBC algorithm in term dose coverage of PTV and dose to OARs. The behavior of small fields on IMRT is also investigated. Significant difference was observed in percentage Isodose distribution, hotspot, dose volume histograms (DVH) and minimum, maximum, and mean dose in P-lung between Eclipse and PrecisePLAN treatment planning system. Extensive care is proposed during the evaluation of external beam radiotherapy treatment plans. The dose calculation algorithm may influence treatment planning and clinical outcome.

Chapter (01)

INTRODUCTION & LITERATURE REVIEW

Intensity Modulated Radiotherapy (IMRT) has significant importance in this modern era of Radiation Oncology. Computer tomography and other imaging modalities improved the outcome of the radiotherapy. Currently, a lot of research is carried out in all over the world to explore this new advancement. A perfect radiation dose minimum dose to the normal tissues is a challenge now a day. It is established fact that if we increase the tumour dose then probability of tumour control is increased. Normally, the tumour dose is mostly inadequate due to the tolerance limits of organs at risk. In external beam radiotherapy, IMRT allows to control the dose to the OAR's with significant increase in the target dose. It provides the opportunity of both reducing late toxicity and escalating the delivered dose which could direct to improved tumour control and survival. IMRT treatment technique is good palliative care management used for advance Lung cancer [1].

In radiation dosimetry perspectives human body consists of a variety of tissues and cavities which is different from water. To increase the therapeutic advantage of radiotherapy, it is compulsory that the dose to target and OAR's predicted perfectly. The maximum dose to (PTV) while minimizing the dose to OAR's depends on optimization of therapeutic advantage. The capability to recognize and to contour these OARs and target structures calculates the electron densities in vivo on a voxel-by-voxel basis. The combination of improved imaging and beam modulation allow accurate and definite radiation around the targeted tissues. If the dose is inaccurately predicted then dose have increased Normal Tissue Complication Probability (NTCP) rates in escalation trials. The precision in radiation dose to the PTV is dependent on the calibration conditions and reference conditions in a water phantom [2]. Secondly, the calculation of dose at any position in the human body be computed and associated to the calibration dose. These variables have to be considered in dose calculation process are sites, electron density of martial and normalization point of dose [3].

In 1970s, generally, it is assumed that the patient was completely consisted of water. The computed tomography (CT) is now clinically available, to obtain electron density information *in vivo,* which could be applied for radiation dose calculation. This combined with modern computers; provide an opportunity in improvement dose calculation, which explain the complicated physical procedure related with the irradiation of the inhomogeneous tissue [2].

In the whole process of the radiation therapy, confirmation of the accuracy in dose calculation is an imperative assignment and associated quality assurance measures especially in low densities regions. It is highly suggested to split the verifications into benchmark, user's beam data verifications and generic beam [1-4]. The assessment of dose calculation algorithms in external beam radiation therapy (EBRT) is usually based on a number of measurements done in simple geometries for radiotherapy treatment planning systems (TPSs). A study of conservative breast cancer patient was published with eleven different TPS which were included to calculate the dose for tangential treatment setup [5].

Scatter–air ratios concept introduced by Cunningham [6] with the Clarkson sector integration [7]. Generally, the recognized agenda was based on the concept, "Improved Low-Density Parity-Check Codes Using Irregular Graphs" (IRREG) for scatter integration where as the equivalent tissue–air ratio method (ETAR) is computed on the O'Connor rectilinear scaling theorem [8, 9]. The model phantom scatters approach is used for many years [9, 10]. Ahnesj¨o and Aspradakis have been reviewed the recent developments using pencil and point kernels for scatter integration simultaneously with the previous techniques [11, 15] and AAPM Report-85 [2]. O'Connor theorem discussed by Cunningham and Woo [12]. Electron transport between media has been proposed by several authors to explicitly account for changes in, but still it has not been implemented commercially and also discussed the reasons by Keal and Yu [13-14]. Presently, commercial photon dose calculation algorithms are using rectilinear density scaling which is mainly approaching from changes in primary electron transport. Collapsed-cone

convolution technique is advanced models based techniques which handle the primary and scatter dose point kernels separately. O'Connor theorem carried out the two point kernels separately with a rectilinear scaling following with different attenuation [15, 16].

Test packages are developed for the verification of photon beam dose calculation algorithms [17]. The TPS's quality depends on the algorithms. Algorithm is used for dose calculation that provides the dose at a point inside the human body on the bases of the patient information and beam data characteristics. Information of the algorithms can help the consumer to recognize the capabilities and boundaries of the definite algorithms. These problems help to design a Quality Assurance (QA) programs to accesses the algorithm performance. The classification of special structures for density corrections is to be treated as inhomogeneities. For non-CT based planning, these 3-D structures are derived from 2-D contours whereas for CT based planning, the electron density is calculated from Hounsfield Units and converted into relative electron densities. Conversion method of electron densities and averaging should be defined in specific manner. The TPSs handle the electron densities by using the density grids or CT input data. Modern TPSs are used many different types of dose calculation algorithm [18, 20]. Initially, dose calculation models were developed on tabular representation to obtain the dose distribution directly from beam data measurements. With the passage of time, TPS dose computational algorithms have progressively evolved towards more physical based models. The most modern algorithms are closed on the Monte Carlo (MC) approach, where each photon is traced as they interact with matter. In MC and table based models exists a full range of possibilities. In each algorithm, the dose calculation accuracy depends on those quantities which are used by the algorithm. The characteristic and parameters of beam data required varies with respect to model. A larg number of tables are required in measurement based models but in physical based models only a small number of parameters possibly will be needed.

1.1 Dose Calculation Algorithms

Modern TPSs are commonly used the PB algorithms for radiation therapy. In most of cases dose calculation difference with PB and more complicated methods are insignificant. The error in dose calculation with the PB algorithms may significant clinically in metal implants, air cavities and lung tissue. Several parameters are involved to calculate the accurate dose in above mentioned sites with the PB algorithms [21-25]. Clinically, for lung cancer treatment planning most of the time PB algorithms is used. Many authors had been reported that the inaccuracies in dose calculation are higher for high energies in low densities sites. Due to this reason, low energy is mostly chosen to generate the treatment plans for lung Cancer patients.

The PrecisePLAN was known as Render- Plan 3D. Initially, it was developed by W D Renner. Elekta Medical systems purchased this treatment planning system and the algorithms were translated in more modern GUI-like background. Fundamentally, the algorithm has almost the same original code. The dose calculation at point of normalisation is separated into a scatter and primary components. Effective path length (EPL) correction is directly taking into account to the point of calculation to compute the primary component. The contribution of the beam areas, fluence and the distance to the skin surface is required to calculate the scatter component. The scatter and primary components calculations are model based. In PrecisePLAN, only primary component is corrected for inhomogeneity, which affects the dose calculation.

Small field apertures in IMRT define the efficiency of external beam dose calculation algorithms. Individual small segments may not affect significantly, but may encompass due to large number of small fields could therefore cause a significant dose calculation error in the whole IMRT treatment plan. Quality controls can receive benefit from mean dose and problems with small segments may not be important in the IMRT fields if it covered a larger region. But this is not implies in small individual fields. Small target volumes are treated with the small fields which may affect significant amount of the given radiation dose. The dose calculation errors in small field's dosimetery could be a

source of considerable error in overall delivery of prescribed dose. Most of the linear accelerators are calibrated under specific conditions. However, a small field, where the calibration apparatus is not standardized which does not work properly because CPE does not exist. In this case the charges particles deposited the dose, may exit from the radiation field in their path. This energy loss cannot contribute by charge carriers incoming from the neighboring regions. As mentioned above, patient is simulated on a TPS that is normally models the therapy machines, radiation transport and energy absorption in the human body. The models of TPS have their own considerations, reservations and probabilities of error. The accuracy in planned dose depend on uncertainties in radiotherapy machines and dose computational algorithm, and commissioning beam data to configure the TPS algorithm. This issue becomes more sensitive when you are dealing the treatment of the low densities region like lungs.

Currently most of the developments undergoing to generate and collect the correction factors for commercially available detectors. The classification of new phantoms (consist of tissue equivalent materials) and small field dosimetery detectors help us to measure radiation dose for a small fields. The dose measurement for small field and improved software tools for treatment planning systems help to determine the accurate dose distribution in human body.

Chapter (02)

PHOTON INTERACTION WITH INHOMOGENEITY

It is highly desirable that the dose deliver to the cancer patient should be accurate with minimum uncertainty. As a whole preferred accuracy in the radiation dose is 5% to a target volume. But the accuracy of computerized dose calculation should be within 1 to 2%. Traditionally, relative dose calculations errors appear due to the following step;

i) Homogeneous medium
ii) Correction of inhomogeneities

If separated evenly, each of these self-governing components would have to be calculated with less than 1.4% uncertainty. On the whole, uncertainty in the directly computed dose distribution form treatment planning system should not be greater than 2% [4].

For the uncertainty assessment, a lot of assumptions are contributed to calculate the accurate radiation dose deposition in the human body. Precision of dose has been assessed as extensively for low densities sites which impact on clinical outcome. Metallic prostheses are also interesting due to high radiation absorption coefficient and high dose effects in the surrounding. The uncertainty in the dose due to metallic hip prostheses was reviewed in Task Group 63 [33]. Clinically, the effects are not well known, but in general the precision for inhomogeneities should be less than 3%.

If the unrestrained predictability caused by the structures, body contour, and electron density related with particular patients is not accounted. Precise dose calculation together with inhomogeneity corrections is a crucial constituent of radiation dose optimization and investigation of clinical results, particularly for 3D conformal radiotherapy and in addition with IMRT to target and OARs unexposed with radiation before.

2.1 Photon Dose Calculation in Inhomogeneous Medium

Photon energy deposits the energy differently in different tissues depending upon the electron density of the tissue. The surface of patient can get from a Monte Carlo simulation by using a spatial, spectral, and directional distribution of photon fluence incident [26, 28]. Fundamentally, there are two step process of the photon energy deposition in tissue [2].

i) Photons interaction in the medium to transfer kinetic energy to charged particles.

ii) Acquired energy of charged particles deposit in ionization and excitation process along a limited trail.

A linear relationship between dose and Total Energy Released per Unit Mass (TERMA) exist, if the charged particle equilibrium (CPE) is established [29]. These are effectively mixing together into single computation. However, for non-equilibrium conditions at tissue interfaces and beam edges, this relationship do not valid the steps must be more clearly defined.

2.2 Photon Interactions with Tissues

Initially, the photon interactions in tissue are characterized by μ is the probability of a photon interacting per unit distance. It depends on,

i) Energy of Incident photon ; E (MeV)

ii) Density of Tissues, r (g/cm^2)

ii) Effective atomic number of tissue (Z)

A large number of photons in a radiation beam are incident on the human body with average energy **E** (MeV) [30]. Energy fluence is characterized by the number of photons reaching to a point in the human body. The total energy released per unit mass (TERMA) is discussed by Rogers and Ahnesjo [31, 32]. It is known that the KERMA less than TERMA. The kinetic energy unconfined and afterward deposited in the vicinity along the tracks. The

collision KERMAc which is normally less than KERMA. The photons produced in bremsstrahlung events are excluded and do not absorb locally. All these quantities are correlated to mass energy transfer, the mass attenuation by energy fluence and mass energy absorption coefficients.

Three competing interactions are dominated in the ejection of photons from the photon beam in the tissue. The effect is summarizes in the figure (2.1). For absorbers with different atomic numbers (Z), the dominant effect is due to the Compton Effect for different photon energies [2].

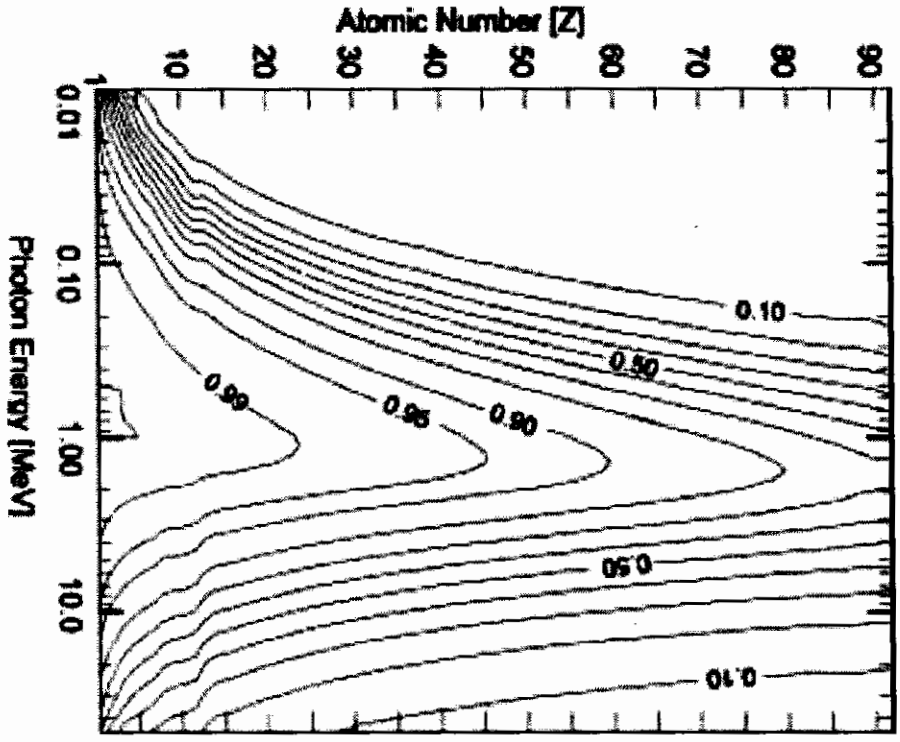

Figure (2.1) Compton scattering as a fraction of photon energy and the atomic number of the different absorbing mediums [33].

2.2.1 Charged Particle Interactions

The photons exchange its energy in recoiling with charged particles, photoelectrons, Compton electrons, and pair production, which are eventually accountable for energy deposited in the tissue. Multiple Coulomb collisions cause to slow down these particles, which deposit of energy in the vicinity in the track and occasionally, bremsstrahlung occurs

away from the track. In the path of a charged, the mass collision stopping power [29] is more important in energy deposition in the neighbourhood down the particle track to combine the energy deposition.

$$S_{col} / \rho = [d\bar{E} / \rho dl] \quad [MeV.\ cm^2/g] \qquad (2.1)$$

$d\bar{E}$ is the average energy and dl is path length. The dependent variables of the mass collision stopping power are charge on particle and atomic number of medium but it is independent from density. For each interaction, charged particles lose an inconsistently disintegrate of energy, but statistically energy straggling [32, 34] is unnoticed and is assumed "Continuous Slowing Down Approximation (CSDA)". A "CSDA range" can be calculated as;

$$R_{CSDA} = \int_0^E [\frac{d\overline{E}}{\rho dl}]^{-1} .dE \qquad [g/cm^2] \qquad (2.2)$$

Then these charged particles are also deflected from their path due to several scattering events, which readdress their energies and cause to change their dose deposition patterns. In higher atomic number materials, this effect is enhanced. The comprehensive computation of these scattering require sophisticated logical or Monte Carlo approach and It has been designed somewhere else for electron beams [28] [34, 44]. However, the particle ranges are considerably longer for higher photon energies and the dispersion of the energy.

2.2.2 Charged Particle Equilibrium

Fractional electron tracks can be balancing to form full ranges within a small volume of interest. If the energy absorbed at the spot the track segments are supposed to be complementary [45]. If true CPE exists, the primary dose becomes precisely equal to the collision KERMA. Basically, CPE is the energy equilibrium in 3D. If the photon fluence is sufficiently uniform a pure equilibrium can develop in the surrounding of the given volume. The charged particles are also released energy uniformly and angular spectrum. From the point of consideration, the adjacent orbits of the atoms consist more than the

lowest thickness equal to the highest range of charged particles commence by the photons. It is only, due to the beam divergence and photon attenuation [46].

Pure equilibrium is difficult to achieve as compared to achieve the Transient charged particle equilibrium (TCPE) [29]. In a uniform absorber, TCPE is attainable along the central ray at depths. It goes beyond the maximum forward range of the particles launched which give the half-width of the radiation field. It also exceeds their maximum lateral equilibrium. In this current situation, attenuation of the bean can be a source of systematic shift of dose and collision KERMA. This absorbed dose is proportional to the collision KERMA. A computation of dose is significantly cut down for CPE and TCPE, since it does not need full tracking of electron trajectories. A lot of easy techniques of inhomogeneity correction were supposed completely CPE or TCPE. It is also helped to avoid dealing with the complication of charged particle transportation.

2.2.3 Atomic Number and Tissue Density

The photon interaction is described by mass attenuation and absorption coefficients are not dependent of mass density. Similarly, the transport of charged particles is described by the mass stopping powers set in motion are quasi independent of density in high density tissues. When dealing standard field of radiation beams and concern linear coefficients of patients are often desired. This density for water-like tissues can be measured easily by using *in vivo* x-ray computed tomography [47-48]. But it can be approximated for indefinite atomic number of tissues, such as bone [50].

Radiation transport explained by two main theorems, O'Connor and Fano [51, 52]. These theorems allow handling the densities for water like mediums with subjective densities. These theorems also present good approach into the problem of different density. It should't be implemented without distinguishing their fundamental natural supposition. These theorems have imperfect application to inheterogeneous since both density and atomic composition might change concurrently [53].

The same consideration is also implicitly developed in Fano's theorem that strengthen the

charged particle equilibrium; occasionally the above mentioned requirement has been inconspicuous and ignored [54]. Between these two theorems, Bjarngard [55] were investigated and incorporated theoretically the common fundamentals and relations within a common framework. At the field edge TCPE is affected by density as compared to central axis values of photon fluence and dose. The density of irradiated tissue can also affect the penumbra of the radiation beam [56]. In low density medium, the field edge is distorted due to the high lateral scatter, as revealed in figure (2.2). The penumbra width (80%–20%) was measured 2.4 times for 18MV photon energy in lung density equivalent phantom than in water phantom, but for 4 MV beam, this size to some extent is lesser in the low density region [57].

In 3D conformal radiotherapy, this penumbral change consequence should be precisely considered to confirm the coverage of PTV [58]. This effect becomes more sensitive in the situation of several overlapping radiation fields.

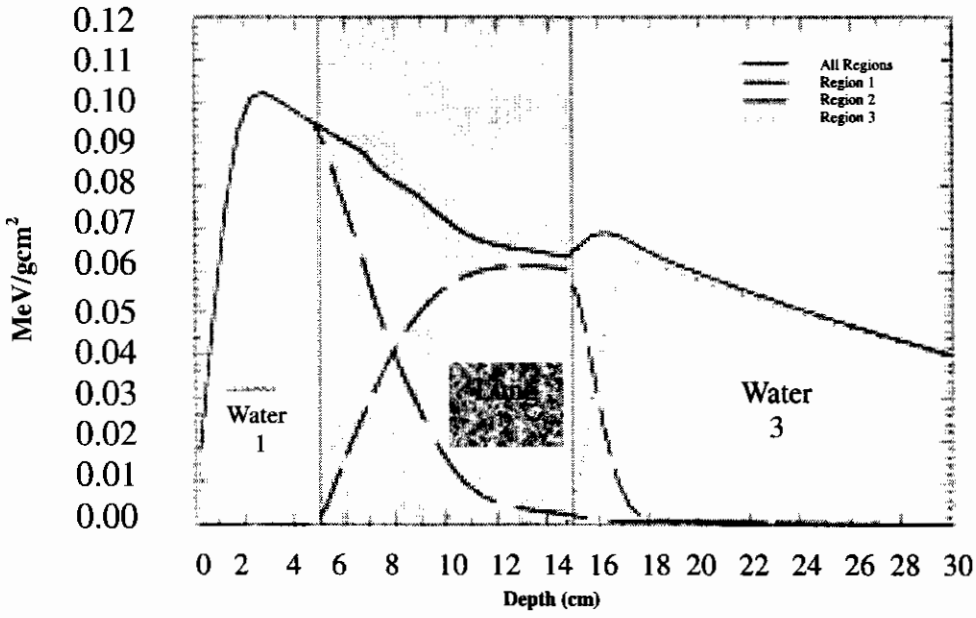

Figure (2.2) Study of high energy, small field and lung inhomogeneity corrections based exclusively on photon fluence [57].

The dose pattern in inhomogeneities is followed by the following factors:

- Interaction of the photon
- Mass attenuation coefficient
- Mass energy absorption coefficient
- Higher atomic number

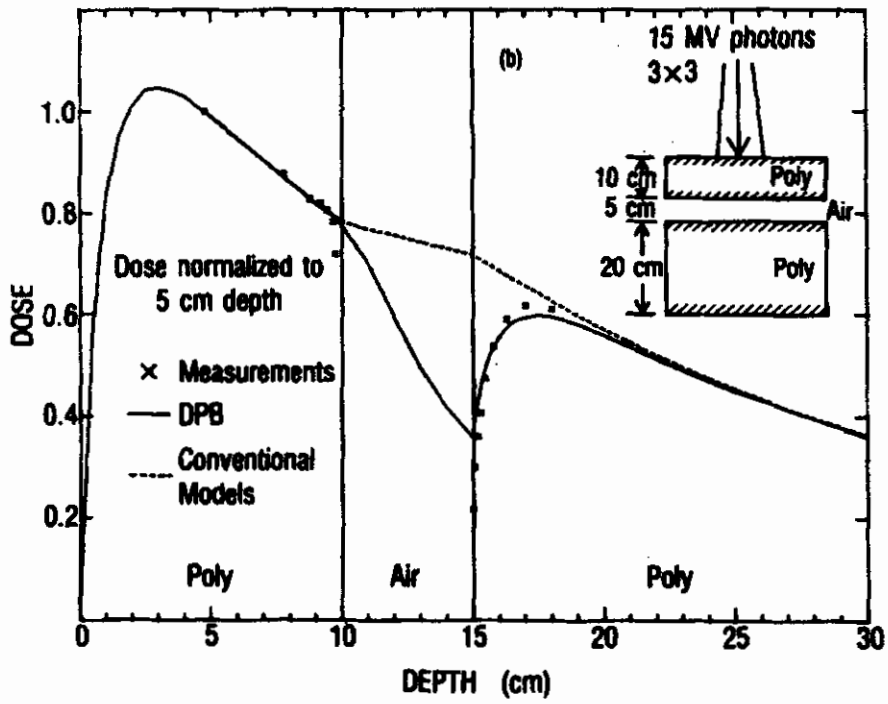

Figure (2.3) At the interfaces between different mediums a considerable electronic non-equilibrium effects take place for same fields sizes as the range of electrons [49].

The most common explanation of heterogeneity corrections reports for alteration in effective atomic number and electron density. It is traversed by primary and scattered photons and charged particles. Compton and Coulomb interactions are dominant in soft tissues. The most important parameter is the electron density of tissues and has merited the high attention. However, sometime particular considerations are required for elevating the atomic number for bone or metallic prostheses, specifically for high photon energies which are greater than 10 MV [33].

2.3 Primary and Scattered Dose Components

Incident photons and scatter electrons (The primary and secondary particles) exert their influence over a different range on the dose. The tissue inhomogeneities and beam boundaries affected individually to different level. In general, empirical and conventional dosimetry instrumentations help to separate these dose components. Recently, Monte Carlo simulations separately defined the "primary" and "scatter" dose component [59]. The dose to the central axis from primary photons at particular depth in the water phantom is depending on:

- Source to Skin Distance
- Machine Head-scatter
- Photon beam attenuation

The dose participation from primary photons is computed by the collimator adjustment in treatment head at any depth and the size does not affect the radiation field at this paticular depth [60]. Initially, photons add the dose due to recoil the electrons in the medium. The dose deposited by photons which interacted at least once in the medium is known as scatter component of dose. Basically, scattered photons dose depends upon the energy of incident photon and the irradiated volume of patient. The total dose is the summation of the primary and scatter dose components.

$$D\,(x, \mathrm{r}) = D_p\,(x) \times (D_s\,(x, \mathrm{r}) \qquad (2.3)$$

Whereas r is the radial distance from the field edge. The primary dose is due to the primary collision KERMA only. It is deposited the dose due to the charged particles. Secondary radiations, including Compton scattered, annihilation, and bremsstrahlung cause the scatter dose. If equilibrium pencil beam is considered for small field size (0×0) cm^2, then scattered photons can considered as due to scattered component [59], as shown in figure (2.4). The stretch of energy is shown in Figure (2.5). The contribution of dose in each component is purely the combination of all pixel values in each dose spread by using the reciprocity theorem [30]. The results of such a computation [56] [61, 62] is shown in figure (2.6) and

point out the comparative significance of all interactions for a 1.25 MeV and a 6 MeV radiation beam.

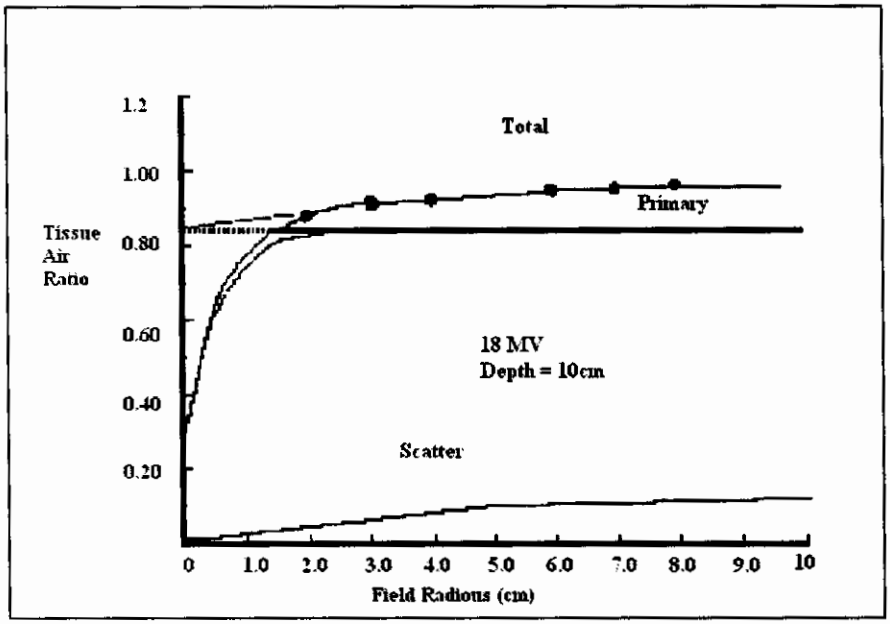

Figure (2.4) Tissue-air-ratios is a function of field radius **r** for an 18 MV photon beam at 10 cm depth in water [59].

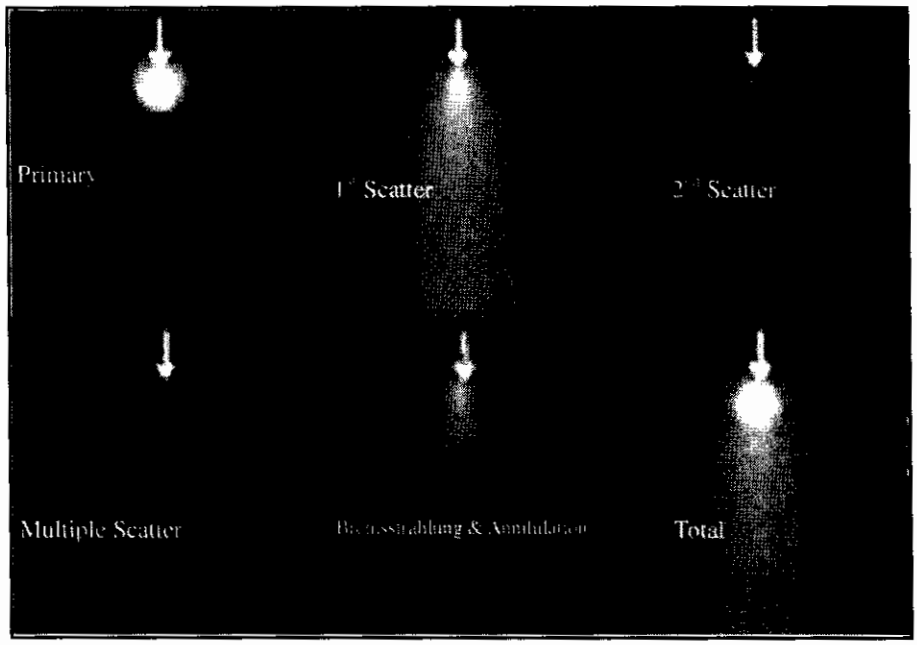

Figure (2.5) Intensity map of Primary 1st Scatter, 2nd Scatter, Multiple Scatter, Bremsstrahlung & Annihilation and total dose map in water for 6 MeV photon pencil beam [56].

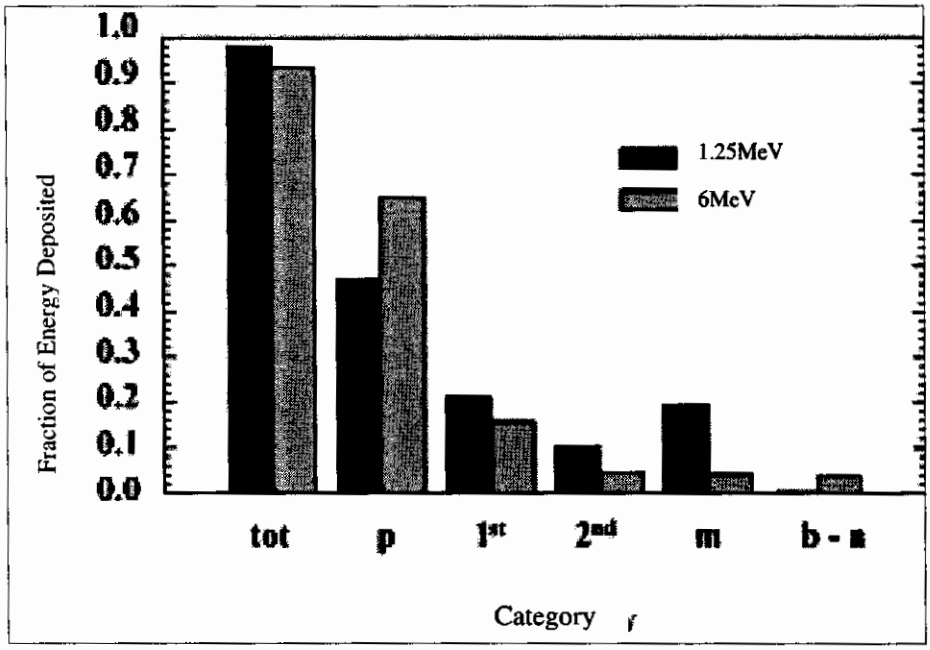

Figure (2.6) The relative importance quantification of all interaction processes (for a 1.25 MeV and a 6MeV beam) [61, 62].

2.4 Inhomogeneity Correction Methods

Experimental validation of dose calculation models is an important step before the implementation of these algorithms in a clinical setting. Suggested dose accuracy for commissioning of treatment planning systems is typically 2% / 2 mm in the high dose and penumbral regions, respectively, in homogeneous phantoms. These criteria are increased to 4%/4 mm in the presence of 3-D inhomogeneities [63], where conventional dose algorithms do not offer explicit electron transport that is usually required to accurately characterize the perturbative effect of the inhomogeneity. The appearance of model based dose calculation algorithm, such as the convolution, superposition and Monte Carlo methods, provide a more physics based approach that has been found by many investigators. These methods are more accurate than correction-based methods for dose calculation in the inhomogeneous medium [64–67].

Dose calculation methods can take two general forms [68] that account for tissue density variations. Conventionally, a comparative dose distribution is computed by considering human body consisting of homogeneous water equivalent. To make the adjustments of

Inhomogeneity Correction Factor (ICF) is applied which due variations in tissue density. The ICF is formulated as:

$$ICF(r) = \left[\frac{\text{dose in heterogeneous medium}}{\text{dose at same point in homogeneous medium}} \right] \qquad \textbf{(2.4)}$$

On the other hand, dose in a heterogeneous medium at a point can be calculated directly using a radiation transport model that would yield absolute dose. Relative dose distributions to a reference point can be constructed by normalizing. A dose distribution is divided on three steps;

- The computation of dose in a water equivalent material which sufficiently replicates beam data measured in water.
- The tissue density and effective atomic number must be provided.
- The relation of variations in tissue density and atomic number is required in inhomogeneity correction method.

These components are complicated to split and these are intricately linked. Inhomogeneity corrections mostly engage the latter two steps to the patient which are mentioned above. In the current era, most of the Radiotherapy centre should have three-dimensional (3D) patient density information [69, 73]. But still many cancer patients are planned on 2D single-slice input data. A primary beam ray tracing procedure is adopted for 2D or 3D density detail in every correction methods. The changes in TERMA or photon fluence is integrated a clear dose computation to every point within the human body due to continuous variation of density. These techniques diverge mostly in a particular manner and tackle the scattering of primary electrons and 3D density information of human body. Schematically, it is shown in the figure (2.7).

In the literature, many authors categorizing the inhomogeneity correction methods according to different criteria. The current techniques separately classify according to their capability to handled primary TERMA and electron transport and whether the human body is being model along 1D primary rays or 3D. The performance of the of the dose computation affect due to the provided information of the human body.

Chapter (03)

PHOTON DOSE CALCULATION ALGORITHMS IN EXTERNAL BEAM RADIATION THERAPY

3.1 Computerized Treatment Planning and Dose calculation Algorithms

In external beam radiotherapy Computerized TPSs are used to create beam profile and calculate the dose with the objectives to increase target dose and reduced the OARs complication. Patient body structure and tumour target can be characterized as 3-Dimentional model. The complete course of treatment planning incorporate numerous steps and on the whole enhancement of the computerized TPS. This is to build up the correctly produce dose distributions and related manipulation. Beyond 1970s, treatment planning was usually done via manual calculation of isodose graph on to patient body outline. The advancement in the CT helps to improve the computerized treatment planning since 1970.

Consecutive enhancement in treatment planning hardware and software remained important in the graphics based dose computation and optimization feature of present TPSs. Some systems utilize the virtual patient in a technique called forward based treatment planning and often equipped with a technique named 'inverse treatment planning'. In the later technique the, system work on user defined setup and optimize dose according the requirement with having total dose being administrated.
After optimizing treatment plan, a dose delivery technique named IMRT is used to calculate the dose to the target and reasonably reduce the dose to OARs. These emerging TPS effectively using the computer aided assistance to increase their throughput.

The correction in homogenous or heterogeneous medium usually with relation for the difference between the typical beam geometry and field size focus on a phantom (water phantom). Beam obliqueness and areas at which the beam does not overlap the patient's body will influence the dose sharing. The patient CT data set is used to

compute the electron density of irradiated volume. Many TPS algorithms make use of either a correction factor or a model based scenario to capitalize on. Model based method [74-89] such as the differential SAR method, accurate model base, convolution or superposition techniques and Monte Carlo based algorithms simultaneously calculate the transport and scatter components. Many techniques are mainly having difficulties with dose manipulation at tissue interaction.

3.2 Dose Calculation Algorithms

3.2.1 History of Computerized Treatment Planning Systems

The algorithms used for dose calculation are the most significant constituent in computerized TPSs. These algorithms are accountable for the correct dose calculation in the human body. The 2-D dose calculation is evolved into partial 3-D point dose kernel methods and then summed up to a complete 3-D dose models.

In the modern TPSs the dose distribution is carried out with 2-D commissioning data in water. The percentage depth doses (PDDs) along the central axis and several OARs (profiles) on certain depths has comprised matrices. To accelerate the dose calculation, central axis PDD interpolate in infinite PDD profiles. Due to this reason, beam data influenced and search the data to generate the dose distributions. On the other hand, they do not represent the 3-D scattering in the human body. CT is extensive use in treatment planning. Irregular field dosimetry was done by using Beam Eye Views (BEV) or simulation films of the fields. By applying the central axis and beam data sets, the primary and scatter parts of the beam is divided using the zero area scatter–air ratio (SAR) and tissue air ratio (TAR) at depth to create Clarkson [6] segments to manipulate at points of concern in the field.

3.2.2 Photon Dose Calculation Algorithms

The photon dose computation algorithms used in TPSs. In the recent development in computer technology, the execution of this method is constantly developing. It is important to know the basics of manual dose calculations before to work on most complicated TPS, [80-82]. The ICRU Report No. 42 [19] discussed the dose calculation algorithms.

Most of the algorithms split the primary and secondary parts and handle separately. In this approach, change in scattering depends on the field shape, intensity and human geometry. A model utilizes convolution approach to calculate the dose in the medium at any point. These models can be administrated as the accumulation of the primary and scatter parts. Such models utilize superposition ideology to explore the variation in the primary fluence and the extention of energy via nearby scattering due to the medium and beam arrangement. The convolution can be used to make straightforward and do rapid manipulation under definite situation of non-divergent basis and uniform phantoms, Monte Carlo or arbitrary sampling methods are utilized to produce dose distributions by subsequent the histories of a enormous number of elements as they come out through the resource of radiation and go through several scattering via inner and outer surface of human body.

The analytical method formulated by Sterling. The dose in the medium is the product of two equations. In which one model the PDD and other model the beam's off-axis parts. It also model shield area of the field size and wedge. TPS formulated in the 1970s to start utilizing the diverged matrix technique of beam administration based on calculated data. The Milan–Bentley model was applied to manipulate diverging in the fan lines that exposed from a source and intersect depth isolines present at preferred distance behind the patient's body. Dose distributions are computed by fast calculating data sets composed of PDD at the central axis and OAR data sets saved via function of field size. This method is persistently in use in treatment planning algorithms [83]. Even though it suffers from the apparent drawbacks of this is required enormous quantity of calculated data, which from their partially availability to correctl scatter model and electron transfer situation. Plain calcification is done between the photon doe calculation algorithms.

A) Correction Base Algorithms

These Algorithms are semiemperical. They are based primary on measured data obtained in a water phantom. Various corrections in the form of analytical funtions or factors are applied to calculate dose distributions in a patient. The correction typically consist of

- Attenuation correction for contour irregularity

- Scatter Corrections is a function of the scattering volume, field size, shape, and radial distance
- Geometric corrections for source to point of calculation distance based on inverse square law
- Attenuation correction for tissue heterogeneities based on radiologic path length (unit-density equivalent depth)

Correction based algorithms represent a verity of methods ranging from those that simply interpolate measure depth dose data to specially formulated analytic function that predict the various correction factor under specified conditions. The dose at any point unusually analysed into primary and scattered components, which are computed separately and then summed to obtain the total dose. Following two equations (3.1 and 3.2) [82] are examples of the calculation that measured quantities such as percent depth dose, tissue air ratio, tissue maximum ratio, and Clarkson method of the integration for any shaped field.

$$\overline{TAR} = TAR(0) + \overline{SAR} \qquad \textbf{(3.1)}$$

and

$$P(d, r, f) = 100[K_p \times TMR(d,0) + \overline{SMR}(d, r_d)] \times \frac{1}{1 + \overline{SMR}(t_0, r_{t_0})} \times \left(\frac{f + t_0}{f + d}\right)^2 \qquad \textbf{(3.2)}$$

Contour corrections and tissue heterogeneity correction are made a part of the correction based computer algorithm for the calculation of dose deposited at a point in a patient. Accuracy of correction based algorithms is limited for 3D heterogeneity corrections in lung and tissue interfaces, especially in situations where electronic equilibrium is not fully established [82].

B) Model Based Algorithms

A model based algorithms computes dose distribution with a physical model that simulates the actual radiation transport. Because of its ability to model primary photon energy fluence incident at a point and the distribution of energy subsequent to primary photoninteraction, it is able to simulate the transport of scattered photons and electrons away from the interaction site. A class of model based algorithms, called convolution superposition, has been underdevelopment since the mid-1980s [31], [65], [84, 86].

- **Convolution Superposition Methods**

A convolution superposition method involves a convolution question that separately considers the transport of primary photons and scatter photon and electron emerging from the primary photon interaction. The dose $D(\vec{r})$ at a point $\vec{r}$ is calculated by:

$$D(\vec{r}) = \int \frac{\mu}{\rho} \Psi_p(\vec{r}') A(\vec{r} + \vec{r}') d^3\vec{r}' \qquad \textbf{(3.3)}$$

$$D(\vec{r}) = \int T_p(\vec{r}') A(\vec{r} + \vec{r}') d^3\vec{r}' \qquad \textbf{(3.4)}$$

Where **μ/ρ** is the mass attenuation coefficient, $\Psi_p(\vec{r}')$ is primary photon energy fluence, and $A(\vec{r} + \vec{r}')$ is the convolution kernel. $T_p(\vec{r}')$ is called TERMA. TERMA is analogous to KERMA, which represents the Kinetic energy released per unit mass in the form of the electron set interaction site. The product of TERMA and the dose kernel when integrated (Convolved) over a volume gives the dose $D(\vec{r})$ as given above in equation (3.3 and 3.4). The convolution kernel, $A(\vec{r} + \vec{r}')$, can be represented by a dose spread array obtained by calculation or direct measurement. The most common method is the Monte Carlo which help you to calculate the convolution kernel, $A(\vec{r} + \vec{r}')$.

A convolution ewuation when modified for radiologic path length (distance corrected for electron density relative to water) is called convolution Superposition equation.

$$D(\vec{r}) = \int T_p(\rho_{\vec{r}}.\vec{r}') A\{\rho_{\vec{r}-\vec{r}'}.(\vec{r} - \vec{r}')\} d^3\vec{r}' \qquad \textbf{(3.5)}$$

Where $(\rho_{\vec{r}}.\vec{r}')$ is the radiologic path length and $\rho_{\vec{r}-\vec{r}'}.(\vec{r} - \vec{r}')$ is the radiologic path length from the site of primary photon interaction to the site dose deposition. The dose kernel $A\{\rho_{\vec{r}-\vec{r}'}.(\vec{r} - \vec{r}')\}$ can be computed by using range scaling by electron density of the Monte Carlo generated kernel in water.

- **Direct Monte Carlo**

The Monte carlo technique consist of a computer program (MC Code) that simulates the transport of millions of photons and particles through matter. It uses fundamental laws of physics to determine probability distributions of individual interactions of photons and particles. The larger the number of simulated particles, the greater will be

the accuracy of predicting their distributions but if you increase the accuracy you need more time to compute it. So the challenge in writing an MC code is that of being able to use a relatively small sample of randomly selected particles to predict the average behaviour of the particle in the beam. The dose distribution is calculated by accumulating (scoring) ionizing events in voxels that raise the energy deposition in the medium. It is estimated that the transport of a few hundred million to a billion histories will be required for radiation therapy treatment planning with adequate precision.

Monte Carlo techniques model particle interactions more accurately by considering the geometry of individual linear accelerator, beam collimating devices and body contour and tissue inhomogenities.

3.3 Pencil Beam Convolution (PBC) Algorithm

The pencil beam algorithm is dose calculation technique. It assumes that any collimated photon beam incident on the patient is actually a conglomeration of lots of smaller, narrow "pencil beams". Each of these pencil beams has a central axis ray along which it deposits some dose. The dose deposition pattern varies with the intensity and the spectrum of the beam that is incident on the patient. The arrangement and weighting of the pencil beams is defined by the field shapers (linac jaws, blocks, multileaf collimators). Where the linac beam profile is non-uniform or modulated (e.g., IMRT) the weighting of each pencil beam is adjusted appropriately. In practice this weighting includes the primary photon intensity at the entry point on the patient and also electron contamination. The total incident energy in the pencil beam is referred to as the primary energy fluence.

This pencil beam will have a very small diameter on the surface (a wise guy might say it could be infinitesimal!). When that pencil beam hits the surface, there will be dose deposited under the surface of water phantom. That dose will have a definite spatial distribution in the water, and it will happen according to the basic scattering and absorption processes that the photons and secondary electrons undergo. This tear-drop/pear-shaped distribution of dose arising from a pencil beam incident on an absorber is referred to the *pencil beam dose kernel* or basically the *dose kernel.* For

our purposes the dose kernel can be thought of as simply the isodose plot arising from one infinitely narrow pencil beam of photons. While in principle it might be possible to set up an experiment with a very small collimator and use very small radiation detectors to map out the resulting dose distribution in water, or some other phantom material, in practice this is a complex undertaking. A Monte Carlo simulation is more common and accurate approach to calculate the dose distribution from a pencil beam in water. These simulations also allow us to generate dose kernels for different photon energy spectra very easily.

In order to get the dose distribution for the whole radiotherapy beam we need to add up the dose contribution to each point from each of the adjacent pencil beams which make up the whole beam. The volume of the patient is divided up into dose voxels and the tabulated dose values for each pencil beam kernel are superimposed on these. At each voxel in the volume the dose contribution from all the surrounding pencil beams is summed up to yield the total dose at that point. This calculation process is called superposition.

In the simplest situation where the dose kernels are all considered the same (ie no change of kernels to account for different photon spectra at different points in the beam) and the patient is considered to be uniform density a mathematical shortcut called "Fourier transform convolution" can be applied to speed up the superposition calculation of the dose. For the more general situation however this approach cannot be followed and superposition must be calculated by applying each pencil beam to the dose voxels one by one and adding up the total dose in each voxel.

Real patients have different densities (bone, lung, airways, muscle, etc.). Different densities lead to different photon attenuations and dose absorptions. To be useful the pencil beam calculation needs to take this into account. Based on the planning CT image dataset, the density of each voxel in the patient is known. The pattern of dose deposition for each pencil beam (i.e., the "dose kernel") can be modified to take these density changes into account. Using the total density of all the material between the point of incidence of the pencil beam and the voxel where we wish to know the dose a scale factor is derived to "stretch" or "squash" the shape of the pencil beam dose

kernel. It stretches if the density has been reduced (like with lung), or squashes if the density has been increased (like with bone) in a region of low density the pencil beam dose kernel would in effect be elongated, whereas in a high density region its dimension would contract to account for the higher attenuation coefficient. These corrections are applied to the dose kernel for each pencil beam depending on the local density variations that affect that pencil beam. After that, the same superposition process of summing up the contributions to each voxel from all the nearby pencil beam kernels is followed. Despite these corrections the pencil beam algorithm still suffers from inaccuracies around inhomogeneities. In practice there are many versions of the pencil beam dose calculation process and each commercial treatment planning system will have a slightly different approach but what has been described above are the main conceptual elements of the scheme.

3.4 CIMMINO Algorithm

Gianfranco CIMMINO was an Italian mathematician. He made important contributions to partial differential equations theory and analysis the other branches of mathematics. CIMMINO refined other mathematical benefit, including numerical analysis. CIMMINO influenced by Mauro Picone (1885-1977) developed an early attention in numerical questions, some of which he will frequently resume in the course of his professional career. The solution of linear algebraic systems is an stylish iterative method. It was published in 1938 and is extensively known as CIMMINO's method. This algorithm has endured the investigation of time and is still extensively used, although in customized form, in a broad diversity of technical and scientific applications.

The CIMMINO is basically a row projection method in which the unique linear system is separated into subsystems. In each iteration, it calculates one projection per subsystem. These projections are constructed an estimation to the solution of the linear system. Optimizations of treatment plans based on a physical model which gives dose limitation are fulfilled for the best distribution of dose is acquired. It tries to determine the dose distribution on a biological model having the sophisticated therapeutic merit lacking any *a priori* postulation about the optimal dose distribution [87-89]. An inverse treatment planning technique is based on the physical model. To

create a treatment plan with a reasonable solution the dose distribution in the PTV and OARs is between the prescribed limits. This kind of optimization is called CIMMINO algorithm.

This algorithm is suitable for large systems of linear inequalities solution [90-91] which is a special structure of the practicable issues. For radiation intensity modulation, the CIMMINO algorithm is implemented in 3D with the combination of 2D. Instead of least squares minimization, linear inequalities are used. The CIMMINO algorithm still converges if a constraint is not fulfilled to a weighted least squares solution. The optimization becomes simpler and flexible if certain prescribed dose limits than the use of objective functions.

A dose deposition kernel **H(x,u)** is required in order to implement the CIMMINO algorithm. The precise a systematic formulation of the kernel is unknown. However, estimated kernels for example a discrete convolution kernel can be used [92]. This sort of kernel does not consider the inhomogeneities. But a discrete kernel is unchanged at particular points in the human body at any treatment site. For the data fitting techniques, a continuous approximation approach kernel is introduced which also account the heterogeneities of the phantom and phantom scattering. For the uninterrupted approximation for **H(x,u),** there are several causes of preferring which are explained below;

(i) The solution of the inverse problem the grid can be flexibly changed. The voxels are split into in the human body and the partition into bixels in the treatment space can be changed according to the shape and size of the target. Increase in speed and accuracy of inverse planning algorithms may the combination of this and the next suggestion [93].

(ii) Adaptive, optimal and automatic grid generation becomes possible. It is also recognized that while precision is improved the uniform grid causes instabilities in the in the Fredholm integral equation of the first kind.

(iii) Awareness of this continuous kernel facilitates to compute dose at particular point in a human body. To estimate the treatment plan can be done more precisely. The DVH can be computed by analytically by using

the continuous approximation kernel in excess of the region of interest rather than mathematically computing the dose at several distinct points.

(iv) **H(x,u)** depends simply on the tissues. It is also possible to influence the constraint of the qualified kernel, for example, using major constituent investigation [94] or some morphological techniques so that more accurate estimation is achieved for a particular patient.

(v) The basic integral equation may be solved to apply the more advanced numerical methods.

(vi) As an intermediate step, it is achievable that the influence of the object function during the optimizing is directly associated to parameters of the multileaf collimator (MLC), without determining the intensity distribution. It capable the user to include the collimator scatters and outflow in IMRT.

A continuous estimated expression for a discrete kernel from Fourier basis functions are calculated through the discrete kernel. It is acquired from dose distributions. It can be computed with the Monte Carlo or direct measurements method. Boltzmann transport equation can also be estimated to relate very precise and accelerated analytical dose computational models [95]. In the CIMMINO algorithm, the continuous kernel is executed for dose calculation.

A preferred practicable solution of IMRT plan even though the complete competence of the CIMMINO algorithm was not optimized for implementation on the 3D patient data. It is obvious that up-gradation in control progressions and dose computation will build the CIMMINO algorithm more convergent. The algorithm also gets more flexibility due to different weighting blocks according to their importance. DVH conditions may be precisely incorporated in a modified CIMMINO algorithm [96]. With the integral of $\{\mathbf{H(x,u)}, \boldsymbol{\Psi(u)}\}$ the efficiency of the algorithm can still be enhanced on a ROI as stated in the beginning. In this way, the size of the matrix is decrease and it reduces the computational time.

Chapter (04)

EFFECT OF INHOMOGENEITY AND SMALL FIELDS ON IMRT

Normally, in computerized treatment planning systems are used the inhomogeneity corrections during the dose calculation. A treatment planning system can accurately compute the dose in an inhomogeneity medium by using the sophisticated algorithm. A lot of publications are available in literature regarding inhomogeneity corrections in TPSs. Those treatment planning system which are using pencil beam algorithms with correction based inhomogeneity calculations are identified to undergo from unreliable level of inaccuracies in calculating the dose in the inhomogeneities media.

IMRT is a very sophisticated technique in which high gradients of dose and improving the ability produce better target dose coverage while sparing the healthy tissues around the target. Heterogeneity corrections for IMRT are more complex than conventional 3DCRT because of presence of large number of small fields, heterogeneity and steep dose gradients [2]. Errors in computed dose distributions generate systematic errors, by the inaccuracy of calculation algorithms, and to convergence errors appear due to optimization process, the second depending on both the objective function and the previous systematic errors [97]. Many authors have discussed the lung inhomogenity correction [98, 101] and found 6% inaccuracy.

4.1 Dose in Inhomogeneous Media

Different research groups did the measurements in non-homogeneous phantoms. The data obtained during these measurements were specifically used to access the algorithms for different low and high energies. For head and neck cancer patients, the dose distribution is influenced in a complex manner due to the existence of curvature of body contour, air cavities, and bony composition. The primary transmissions, the range of secondary electrons and the number of photons scattered in different media cause to change the dose pattern. Currently, the change in the clinical dose is not perfectly understood. Different research groups [22], [102,107] explore the consequence of air cavities in tissue equivalent Phantoms on the dose distribution and attempt to develop the standardization.

The commercial inverse planning TPS depend on fast but estimated dose computational algorithms. There are two different errors occur in iterative inverse

treatment planning. One is describing systematic and other is convergence error that comes out during the optimization. The convergence inaccuracy is comparable to the noise which comes out in inverse treatment planning when Monte Carlo (MC) dose calculation engine is used [108,109]. Jeraj et al. [109] has studied different cancer types and tried to differentiate both errors. The systematic error was larger for PB (up to 8%) and for superposition it was found to be 1%. In dose calculation method, the convergence errors rely on the systematic error.

When the final dose manipulation is carried out with a precise dose calculation algorithm it reduces the convergence error. For generating error free treatment plans, the convergence error should be removed during the optimization. In final plan we have to still compromises due to the existence of convergence error that is clinically significant. For the PB algorithm, both errors influenced significantly. IMRT treatment planning should be planned with sophisticated algorithm to reduce the all kind of errors. This reason needs to be considered the cause of IMRT dose calculation algorithms which is in basic 3D CRT Planning system. If comparison is done between significance of accuracy in dose calculation and statistical uncertainty for inverse treatment planning [108,109] that the systematic and convergence inaccuracies for superposition dose calculation algorithm are almost equivalent to 2% statistical error of a MC. Keall et al. [110] reported that to achieve anything by using MC algorithm for IMRT, accuracy of the dose computation should be less than 2% in the final dose calculation.

It is seen from the conclusions, the pencil beam dose calculation has high convergence errors, as one could imagine, depend on the significant systematic errors. The optimizer convergence error was estimated which should be less than 0.5% for target and outside target regions is about 1–2%, which is lesser than the experimental convergence error. Jeraj and Keall [110] also have the same opinion for the convergence error. Convergence errors can also be reduced by increasing the simulated annealing iterations.

In this study it can be concluded that the convergence errors is almost proportional to the systematic errors. Therefore, the convergence error for pencil beam dose calculations algorithm is greater than superposition Algorithm. On the other hand,

different objective functions compel a huge extension in these errors in consequently less. Due to the uncertainty in the description of the optimality, the magnitude of convergence error is uncertain.

4.2 Small Field Size

Presently, a small field is definition very subjective and ***ad hoc*** in radiation dosimetry. Still there is no comprehensible agreement definition about a small field. Generally, all those field sizes which are less than (3×3) cm2 are supposed small fields. These small fields dosimetry and dose computation unusually required special consideration. Small fields are required to adjust the criteria which state the situation based on the beam energy and the medium. There exist three main factors which state the scale if a field size could be considered as small or not [111].

(i) The detector position in the beam aperture and the size of the viewable component of the beam origin as projected

(ii) Detector size

(iii) The range of the electron in the exposed medium.

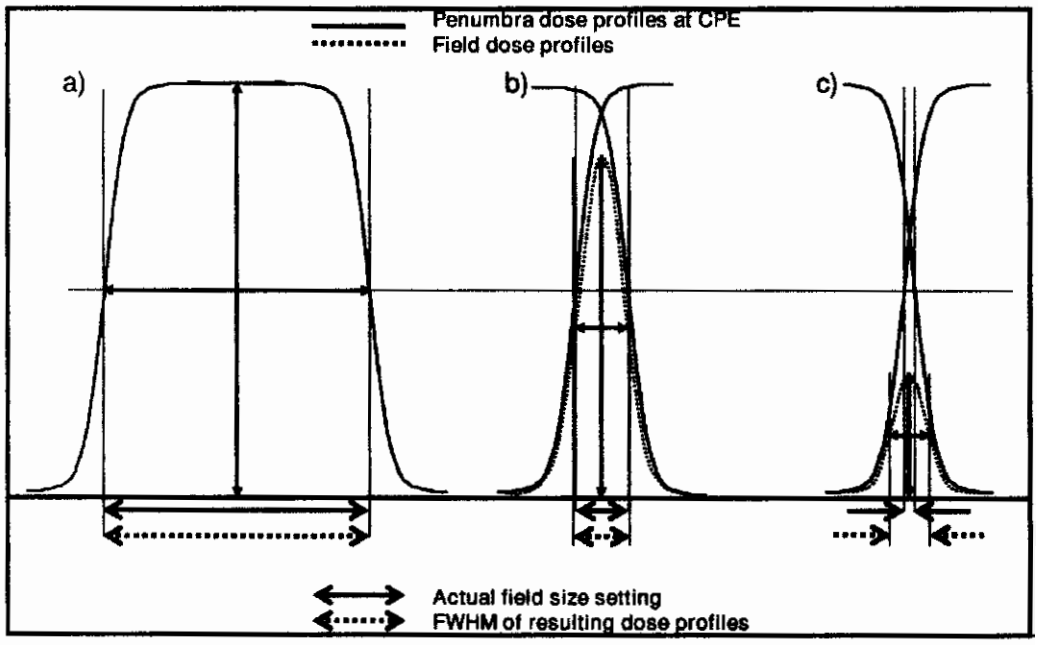

Figure (4.1) The full width at half maximum (FWHM) of dose profiles yields correctly determined field sizes (a). When the field size is of the same order as the charged particle lateral diffusion distance a small error in field size determination from FWHM data (b). Completely break down for very small fields, resulting in an overestimated field size as shown in panel (c) [112, 117].

as compared to field sizes at which the full source can be seen from the detector [112,117]. The output changes are illustrated in Figure (4.1). The geometrical penumbra is extensive all over the field cross section due to the full source cannot be seen from the centre axis of the radiation field. In these conditions conventional methods to determination the field size such as full width at half maximum FWHM break down, overestimated field sizes.

The beam output can be significantly influenced by the secondary collimators adjustments used to attain the small field sizes [118]. It is explain in the figure (4.2), representing the 6 MV beam profile patterns with a range of jaw adjustments. Due to the curved nature of the leaves MLCs the light fields are not matching with the radiation field which allowing the variable quantity of radiation through variable thicknesses of the leaves [119]. It causes variations from one side to the other of the field due the positional dependence, further complicates the specific metrics of small field sizes.

In a low density medium, the electrons range is prolonged at a considerable length which produced from high energy photon beams. For CPE, the lateral range of the electron rather than the forward range of the electrons are the critical parameter compared to the field size.

Energy dependent influenced the lateral range of electrons [120]. For different beam energies, primary dose profiles in water across a collimating edge, specified with quality index (TPR20/10) [121,122] as shown in figure (4.3). It offer the penumbra ranges information in unit density media that adjust the dimensions when small field situation be valid based on overlapping electron distribution region from diverse field edges [123].

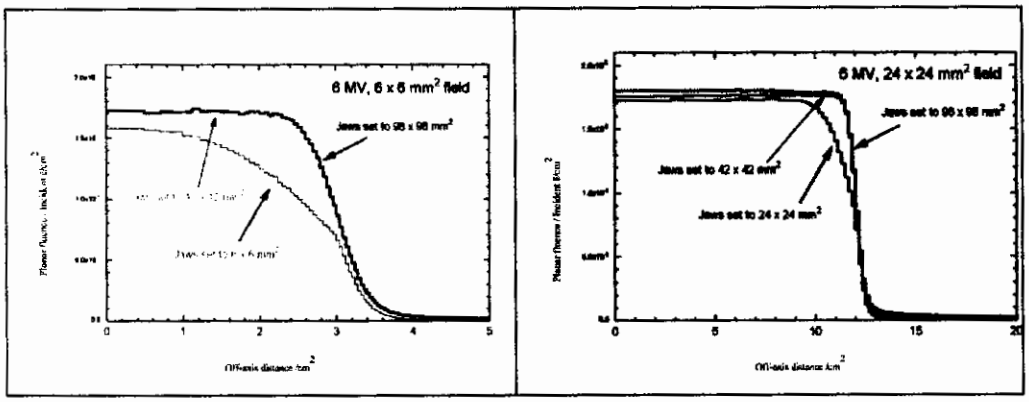

Figure (4.2) The effects of source size and beam shaping geometry on the output of a small field, (a) 0(.6×0.6) cm2 and (b) (2.4×2.4) cm2[119].

Small fields are rottenly used in this modern era of radiotherapy like IMRT and stereotaxy. In radiotherapy, small fields or larger uniform or nonuniform fields that are consisted of small fields are used. It is the main reason for all the clinical treatment beam types including high photon energy, electron, light ion and proton beams. Unusual fields are moreover designed small fields or sometime non-equilibrium conditions exist as discuss in already; this happens, for example, when the field size is close to the size penumbrae [111].

Due to the technological changes in customized linear accelerators have enhanced mechanical accuracy, constancy and dosimetric control. Simultaneously, mini and micro multileaf collimators (MLCs) on conventional accelerators have been an growing availability in the clinic. These developments become a cause to increase the uncertainty in dosimetry and its connect to reference dosimetry based on Codes of Practice.

Due to these reason the dosimetry errors has increased which have become significantly higher than in conventional beams as is demonstrate in various references, including [124, 125] and the disagreements between Monte Carlo calculated and measured outputs with different detectors is shown in figure (4.4).

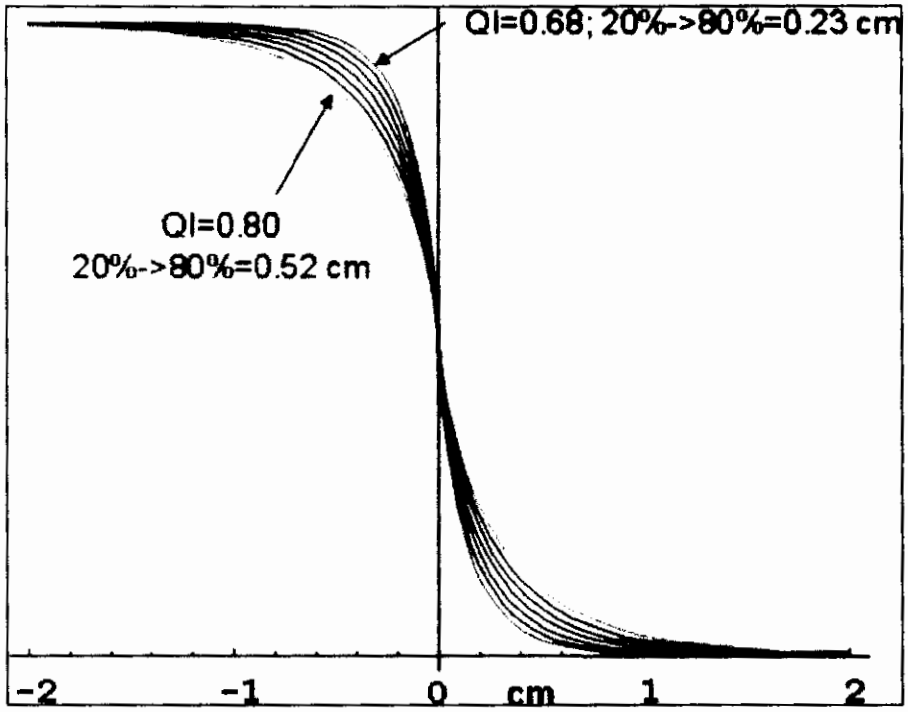

Figure (4.3) The primary dose profile in water across a collimating edge for different beam energies [123].

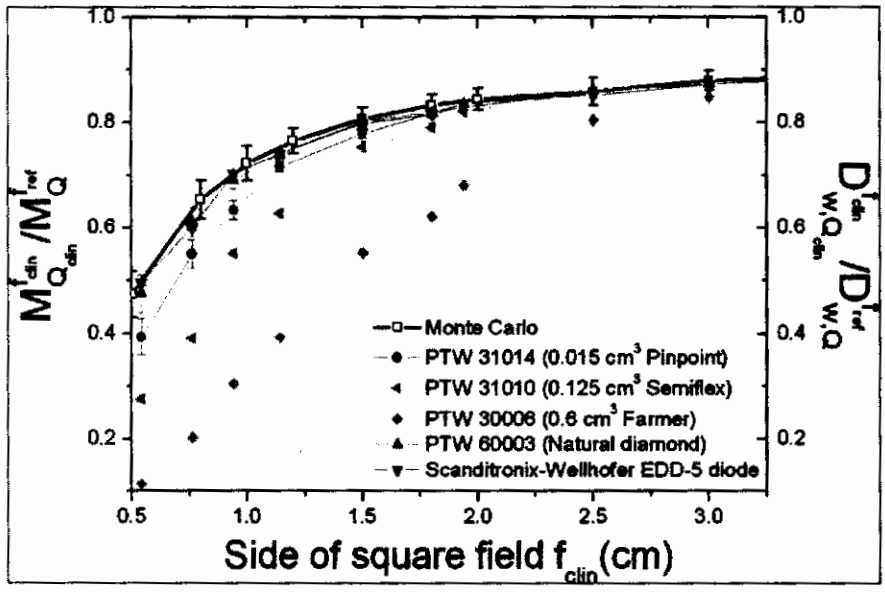

Figure (4.4) Ratios of Monte Carlo calculated absorbed doses to water with different radiation detectors and field size which are normalized for (10×10) cm2 field for 6 MV beam at a depth of 5.0 cm [125].

Chapter (05)

MATERIALS AND METHODS

This study is purely based on computer treatment planning and these generated IMRT treatment plans were only used to study the performance of photon dose calculation algorithms (PBS and CIMMINO) for advance lung cancer patients. In this study, we used the standard CT data sets without respiratory gating and do not consider the respiratory motions. These plans were not clinically implemented on the patients.

The intensions of this study was to evaluate the differences between Pencil Beam Convolution (PBC) and CIMMINO photon dose calculation algorithms in lung IMRT. Investigation of these two external beam dose calculation Algorithms were done on the basses of dose deposition in Lung densities area for low (6MV) and high energy (15 MV), quantify isodose distribution differences with respect to photon energies and furthermore, the influence of small apertures on the dose distribution was investigated in lung densities region.

Before doing the treatment planning, we did the analysis of commissioning conditions for both the treatment planning systems (Eclipse and PrecisePLAN) which are using the PBC and CIMMINO algorithms respectively for IMRT treatment planning. Both treatment planning systems required specific beam commissioning data sets before clinical use. A summary of the equipments used and some measurement parameters are displayed in Table (4.0).

Sliding window optimization technique was used for PBC algorithm and aperture base optimization technique was used for CIMMINO algorithm. We also developed the plan approval criteria for each treatment plans as shown in table (4.1).

Five non-small cell lung cancer (NSCLC) cases were chosen for this research project, with apparent dissimilarity in tumour site. These patients were treated during the 2010 to

2011 in Radiation Oncology Department at Shifa International Hospital Limited (SIH) Islamabad, Pakistan.

Table (5.1) Commissioning information of PrecisePLAN and Eclipse treatment Planning Systems (TPS)

Items	PrecisePLAN 2.15-20.22		Eclipse 7.5	
Machine Commissioned	Precise (ELEKTA)		Varian 2100C	
IMRT Planning Algorithm	CIMMINO		PBC	
Resolution for PDD data	0.2 mm		0.2mm	
Resolution for Transverse Profile data	Field Edges	Center	Field Edges	Center
	1mm	0.5mm	1.5mm	0.5mm
MLC's Type	Curved End		Curved End	
MLC Thickness	1cm (40 pairs)		Millennium 120 (60 pairs)	
Calibration Depth (1MU=1cGy)	6MV = 5cm	15MV = 5cm	6MV= 5cm	15MV=5cm
Calibration Technique	SSD = 105		SAD = 100	
MLC's interleaf Leakage	<4%		<4%	
Detector Size for PDD and Profile measurements	0.13cc (IBA)		0.125cc (PTW)	

The virtual simulation is done on Computer Tomography (SOMATOM Sensation Open 24 Slices) at SIH. Target (GTV) and OAR's (Lungs, P-Lungs, Esophagus, Cord, P-Cord, and Heart) were delineated with the consensus of the Radiologist and Radiation Oncologist. For the planning target volume (PTV), 1cm margin is added isotropically to the GTV. P-Lung was marked as normal lung which included Ipsilateral and Contralateral lung of the patient. It was automatically generated by using the virtual simulation software. Radiation Oncologist also delineated the P-Cord around the spinal cord with extended 0.5cm margin. This extended margin around the spinal cord helped during the treatment planning to control its dose. For IMRT treatment planning, each patient CT data set was transferred according to DICOM RT protocols to both the treatment planning systems (PrecisePLAN, Eclipse) along with OARs and Targets (GTV and PTV) .

Four IMRT treatment plans of each patient were generated. Two treatment plans were generated with CIMMINO algorithms using 6MV and 15MV photon energies on

PrecisePLAN treatment planning system and two more treatment plans were generated of the same patient with PCB algorithms using the same 6MV and 15MV energies on Eclipse treatment planning system. During the generation of these treatment plans, dose constraints for target and OAR's, gantry angles, numbers of beams, point of normalization, total prescribe dose (60Gy), number of treatments, dose per fraction, dose calculation voxal size, mulitileaf collimator (MLC) intrusion (30%) and minimum Monitor Units (MU) per aperture for each treatment plan of the particular patient. CT density file were commissioned in Eclipse treatment planning system before start the treatment planning.

Table (5.1) Treatment Planning conditions and Tolerance Doses limits of OAR's and Target.

Photon Energies	6MV, 15MV	
Total Dose	60Gy	
Number of Fraction	30	
Minimum Aperture Size	(2.5x2.5) cm^2	
Dose Grid Size	0.2cm^3	
Minimum MU Per Aperture	1	
No. of Iterations	Minimum 4000 in PrecisePLAN, and 4000 in Eclipse	
Tolerance of OAR's and Target		
Organ	**Volumes in (%)**	**Doses (cGy)**
P-Lungs	Mean Dose	2000
	<50	500
	<45	1000
	<35	2000
P-Cord (0.5cm margin around Spinal Cord)	0	5000
Spinal Cord	0	4500
Esophagus	Mean Dose	3500
	<30	5500
Heart	<50	3000
GTV	95	95% of Prescribe Dose
	5-10	107%-110% (inside GTV)
PTV	95	95 to 90% of Prescribe Dose
	5-10	107 to 109% (inside GTV or PTV)

During the treatment planning it is also consider that no beam was set through the Contralateral lung.

There were two main reasons to commission CT density file in Eclipse because Shoukat Khanam Memorial cancer Hospital and Research Center did not have the same CT simulator and secondly these patients are simulated on SOMATOM Sensation Open CT simulator.

These four treatment plans were compared on the bases of percentage Isodose, dose volume histograms (DVH) and also did the percentage Isodose comparison of small apertures in the lung density region. Small apertures are normally the part of the IMRT treatment plans. First of all, percentage Isodose distributions were compared of each patient on the two dimensional (2D) CT data sets at central axis slices (Transverse, Sagittal and Coronal). We compared those treatment plans which were generated with same photon energies but different algorithms and then we also compared these two algorithms behavior between high energy (15MV) to low energy (6MV). Similarly, Percentage Isodose Distribution, Hotspot, Dose volume histograms (DVH) and Minimum, Maximum and Mean ($D_{min.}$, $D_{max.}$ and D_{mean}) doses of OARs and targets are compared. The evaluation parameter for PTV included the Homogeneity index (HI). Conventionally, Homogeneity index (*H*-index) is the ratio of the maximum dose in the target to the prescribed dose [135]. A value of Homogeneity index closer to 1 representing better homogeneity of dose in the target. The *H*-index normally fluctuates from 1 to 1.5 in the real treatment plans. In general, homogeneity index has guided to its being broadly used for computing the dose homogeneity in the target. Homogeneity Index (HI) is also calculated for the PTV and evaluated. For the comparison of small apertures, we generated plans with the (3×3) cm^2, (2.5×2.5) $cm^2$and (10×10) cm^2 on only one patient CT data sets and normalized each field in the lung density region at 10 cm depth with Gantry angle zero degree. Prescribe dose was 100cGy in one fraction. Each small aperture was optimized in PrecisePLAN and Eclipse treatment planning system. We tried to investigate the percentage Isodose difference between these two algorithms with respect to depth and also investigated the dose absorbed in the lung density region with respect to the volume of lung by using the DVH.

Due to unforeseeable delays in material acquisition only square fields were studied. A similar study would be interesting to perform for thin elongated fields and various small irregular fields as well. It is hard at this point to say which method would work best and maybe they have to be studied separately. By keeping the geometries simple and studying Small Square fields the comparison and evaluation will be more rigid than for irregular field shapes. The photon energies of available were 6 and 15 MV, so we studied only these photon energies in this thesis. For time restrictions the study was focused on 6 MV and 15MV since it is the common beam energies in use for IMRT while 15 MV is rarely used in lung IMRT clinical applications. But for the sake of algorithms comparison we also include 15MV energy.

The comparison schematic diagram is shown as under;

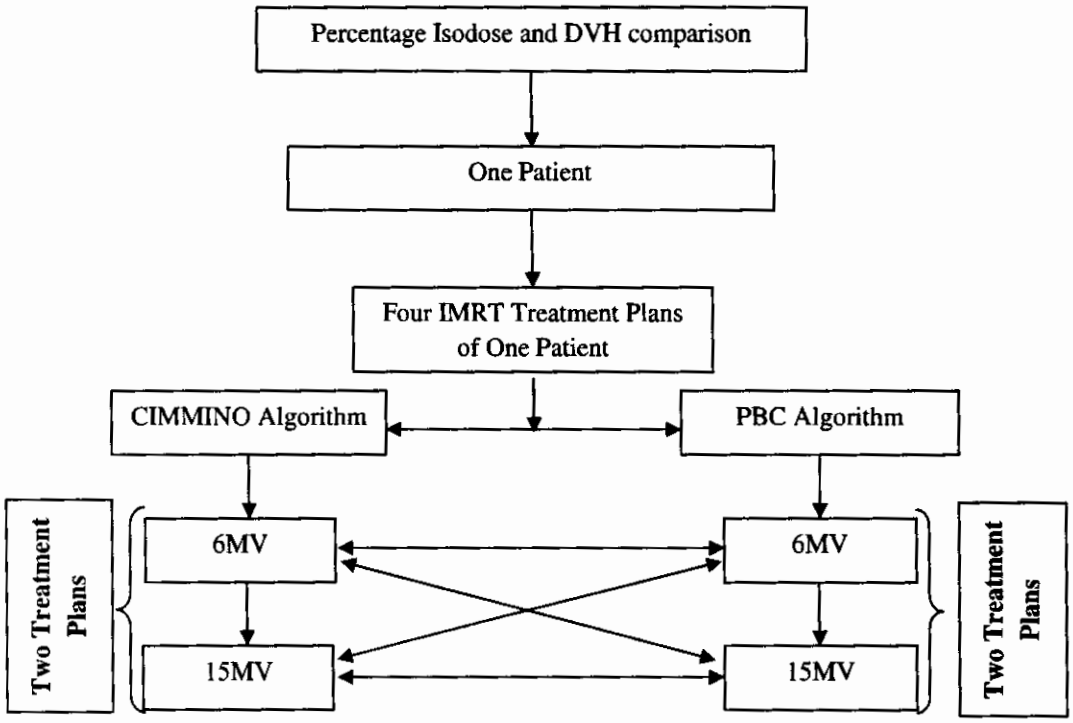

Figure (5.1) Schematic Diagrams of percentage Isodose and Dose Volume Histograms (DVH) comparison between CIMMINO and PBC Algorithms for Lung IMRT treatment plans with respect to Energies.

Chapter # 06

RESULTS AND DISCUSSIONS

In this study, qualitative and quantitative comparison has been done of these two photon dose calculation algorithms in lung Intensity Modulated Radiation Therapy (IMRT). Four different treatment plans of each patient were compared and investigated the dose distribution difference with respect to energies and dose to the lung volume with respect to Target dose.

6.1 Comparison of Percentage Isodose Distribution

6.1.1 Comparison of the 6MV Treatment Plans

The dose grid size was taken 0.2cm^3 to generate the Percentage Isodose distribution. The assessment was done for one patient to make the study simple and clear. Two treatment plans with 6MV photon energy of a patient were generated with the PBC and CIMMINO algorithm. The central axis CT slices of both the treatment plans were compared. The central axis slices of these treatment plans are shown in the figure (6.1). It has been observed that the dose in Ipsilateral and Contralateral lungs, skin and peripheries was high in that plan which was optimized with PBC. This difference was clearly seen if 60%, 50%, 40%, 30% and 15% isodose lines were compared in the transverse slice. Similar behavior can be seen in the Coronal and Sagittal slices of this patient. It was also found that the maximum hotspot at any point in the body and hotspot at central axis slices was higher in that treatment plan which was optimized with the CIMMINO algorithm than the PBC algorithm. Coverage of the target (PTV) was good enough in that treatment plan which was optimized with CIMMINO algorithm then the PBC algorithm.

Similarly, the percentage Isodose distribution comparison is done of remaining four patients. After the evaluation of each patient's treatment plans it was observed that each patient has shown the exactly the same trend which has been discussed above.

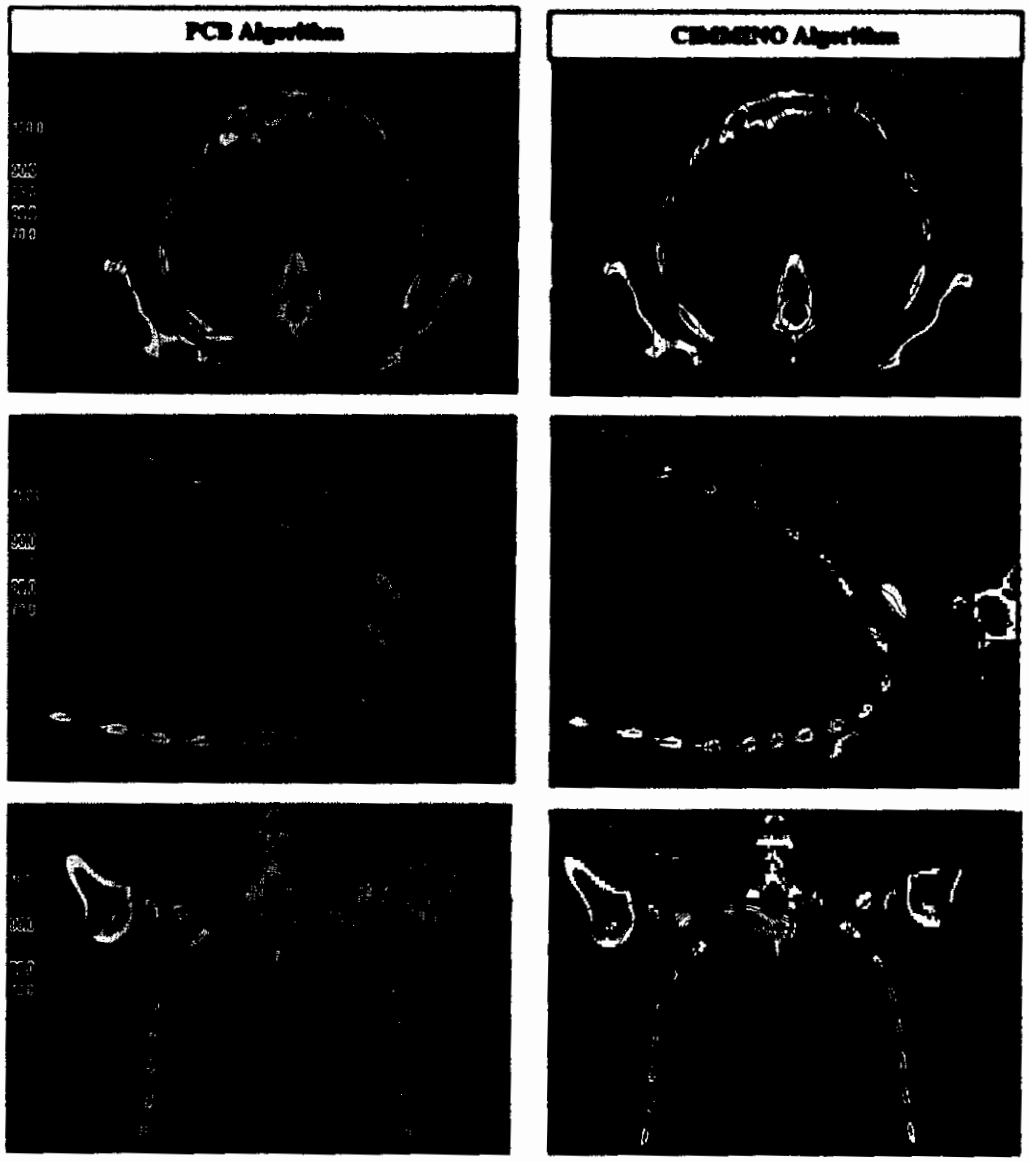

Figure (6.1) The comparison of the Percentage Isodose in Transverse, Sagittal and Coronal Slice of a patient planed with the 6MV Photon Energy and optimized with PBC and CIMMINO algorithm.

But it was also seen in two patients which was planned with the PCB algorithms that 60%, 50%, 40%, 30% and 15% Isodose lines enclosed the very large Contralateral lung volume at central axis slices which is more dominant in coronal slice as shown in Figure (6.2). Hotspot variation was also 3-4% high in central axis slices in those treatment plans which were optimized with the CDMMNO algorithm. The maximum hotspot at any point was higher and target (PTV and GTV) coverage was also better in those treatment plans which were optimized with the CDMMNO Algorithms than the PCB algorithm's treatment plans.

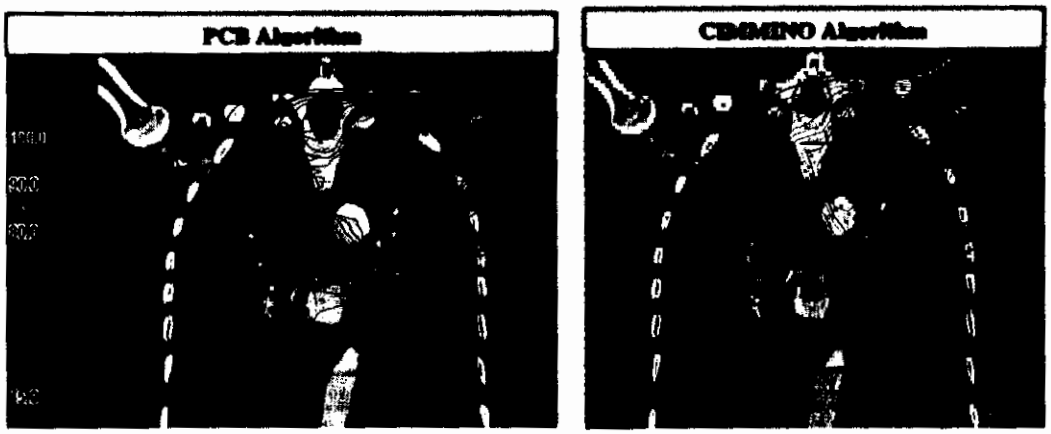

Figure (6.2) The comparison of the Percentage Isodose in Coronal Slice of a patient planed with the 6MV Photon Energy and optimized with PBC and CDMMNO algorithm.

6.1.2 Comparison of the 15MV Treatment Plans

In similar manner Parentage Isodose distribution of 15MV photon energy treatment plans were compared for each patient but overall we got the similar outcome as we had got during the comparison of the 6MV photon energy treatment plans. But some important and interesting effects have been observed during the comparison of 15MV treatment plans. The percentage Isodose distribution was more concentric to the target, sparing the Contralateral lung and depositing the lesser dose in the peripheries and skin in those treatment plans which were optimized with the CDMMNO algorithms than the PBC algorithm.

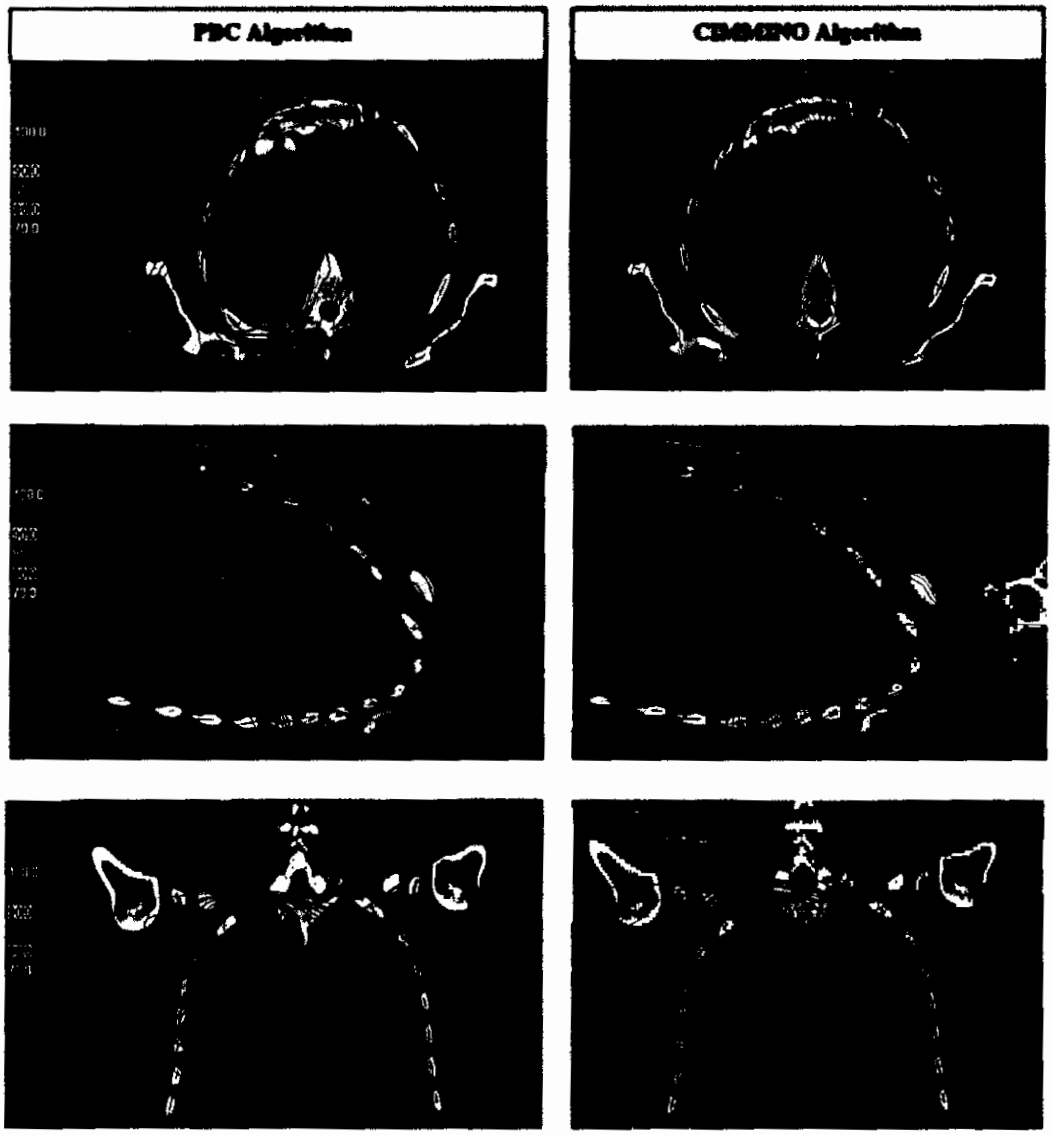

Figure (6.3) The comparison of the Percentage Isodose in Transverse, Sagittal and Coronal Slice of a patient planed with the 15MV Photon Energy and optimized with PBC and CIMMINO algorithm.

In most of the patients the hotspot was similar and within 1-2% differences in central axis slices but in some treatment plans, hotspot was varied up to 6% in Sagittal and Coronal slices in those treatment plans which were optimized with the CIMMINO algorithm. But overall hotspot was higher in those treatment plans which were optimized with the

CIMMINO than PBC algorithms. The comparison of one patient is shown in the figure (6.3). Standard deviation of maximum hotspot at any point in the body in 6MV and 15MV treatment plans is ±1.49 and ±1.7 respectively. Trend of the maximum hotspot is shown in the figure (6.4).

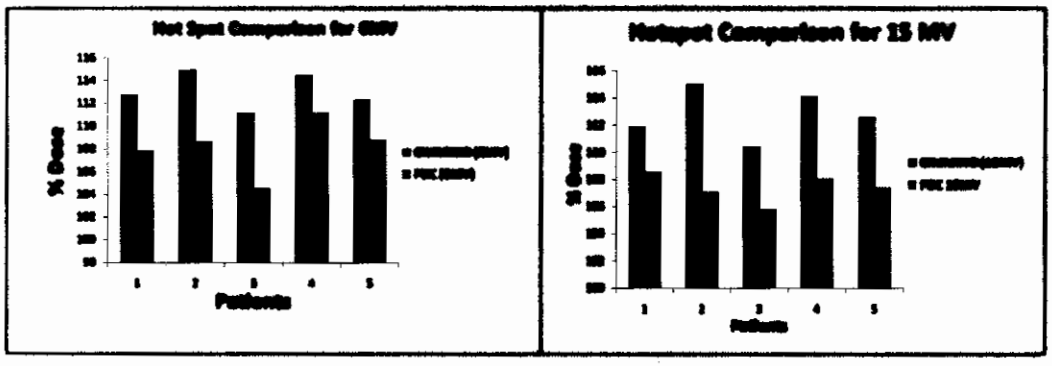

Figure (6.4) The Comparison of the Maximum Hotspot between PCB and CIMMINO Algorithm for 6MV and 15MV treatment plans.

6.2 Comparison of Minimum, Maximum and Mean Doses ($D_{min.}$, $D_{max.}$ and D_{mean})

Comparison of Minimum, Maximum and Mean doses of normal lung (P-Lung), PTV, Heart, Esophagus and Spinal Cord are shown in the figure (6.5). Minimum ($D_{min.}$) and mean doses (D_{mean}) of the P-lung were almost similar and no significant difference had seen in four patients in PBC and CIMMINO algorithm for both the energies. Only in patient (2) it was noticed that the mean dose (D_{mean}) was higher in that plan which was optimized with the PBC than the CIMMINO for both the energies. Significant variation between the minimum ($D_{min.}$) and maximum dose ($D_{max.}$) of PTV had seen in PBC and CIMMINO algorithm plans for both the energies in all patients. But in mean dose (D_{mean}) of the PTV was almost similar. Minimum doses ($D_{min.}$) of the esophagus were roughly comparable with respect to the algorithms and energies but significant disparity in $D_{max.}$ and D_{mean} for both the energies had seen in all patient. Similar trend of this disproportion was also seen in the spinal cord comparison.

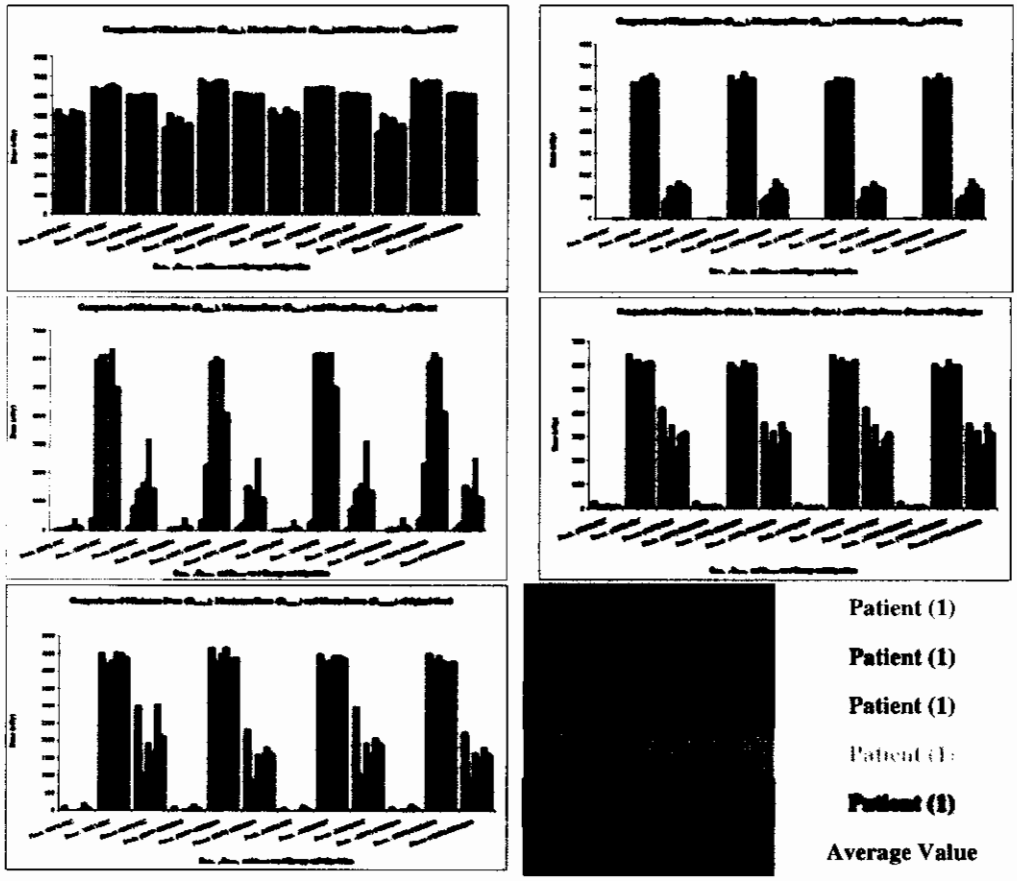

Figure (6.5) Comparison of Minimum ($D_{min.}$), Maximum ($D_{max.}$) and Mean Doses (D_{mean}) and of normal lung (P-Lung), PTV, Heart, Esophagus and Spinal Cord with respect to 6MV and 15MV photon Energies and PBC and CRMMNO algorithm.

6.3 Comparison of Dose Volume Histogram (DVH)

DVH difference was plotted for PTV, P-Lung, Esophagus, Heart and Spinal Cord in DVH for those treatment plans which were planed with the same energies but different algorithms. PBC algorithm was taken as a reference to calculate the difference in DVH.

Planning Target Volume (PTV)

PTV dose coverage was slightly higher in CRMMNO algorithm between 0 to 95% volumes. . The dose coverage was significantly lower from 95% to 100% volume for both the photon energies in patient (1) and (2) only as shown in the figure (6.6).

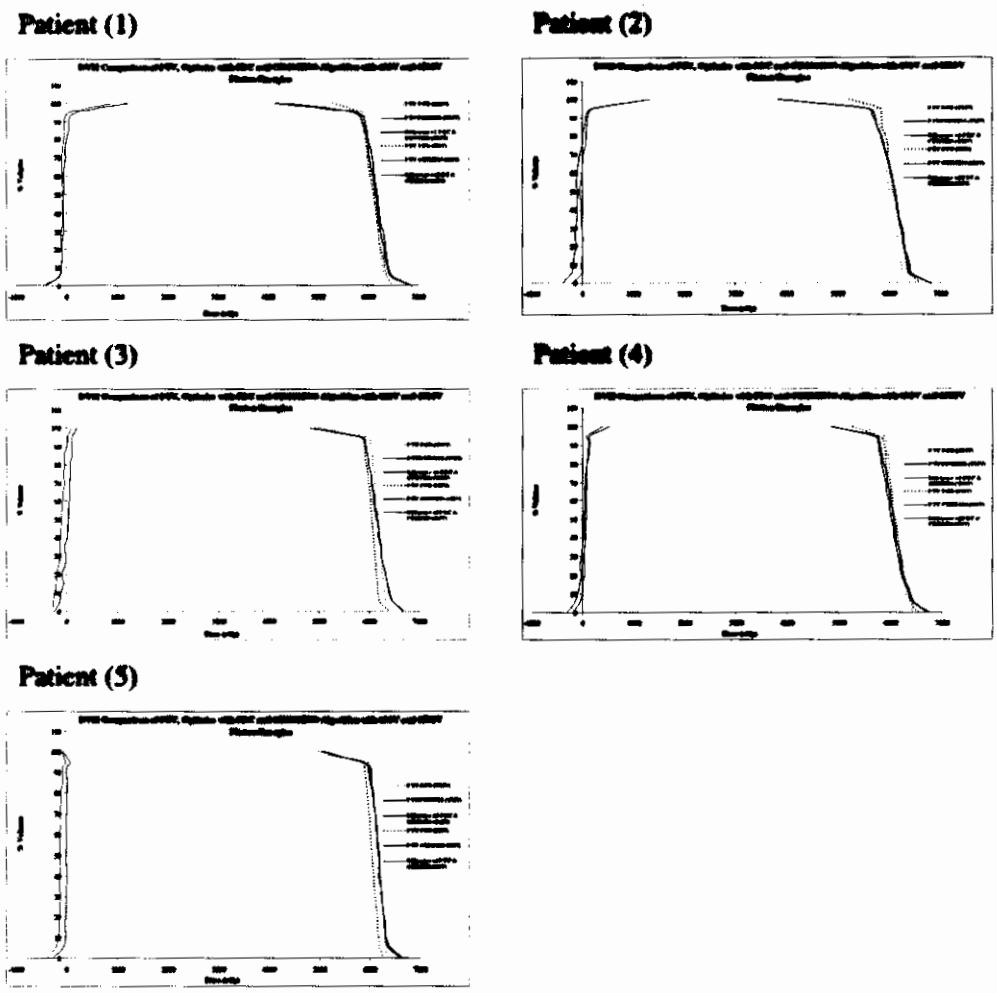

Figure (6.6) DVH and dose difference comparison of PTV between PBC and CIMMINO algorithm for 6MV and 15 MV photon energies treatment plans.

DVH difference in 6MV and 15MV treatment plans was slightly different from 0 to 100% volume of PTV. These treatment plans which were optimized with the PBC or CIMMINO algorithms were showing slightly different DVH difference of PTV for both the photon energies in all patients.

Homogeneity Index (HI) of PTV was close to 1 for 6MV but average value for 15MV is 1.069 which is little bit higher than 6MV for PBC algorithms. For CIMMINO algorithm the percentage difference of HI of PTV was 0.14% between 6MV and 15MV photon

energy. Percentage difference of the average value of the HI of PTV of five patients between PBC and CIMMINO algorithms for 6MV and 15MV is 11.86% 6.04% respectively. Homogeneity Index for PBC and CIMMINO algorithm is graphically presented in figure (6.7).

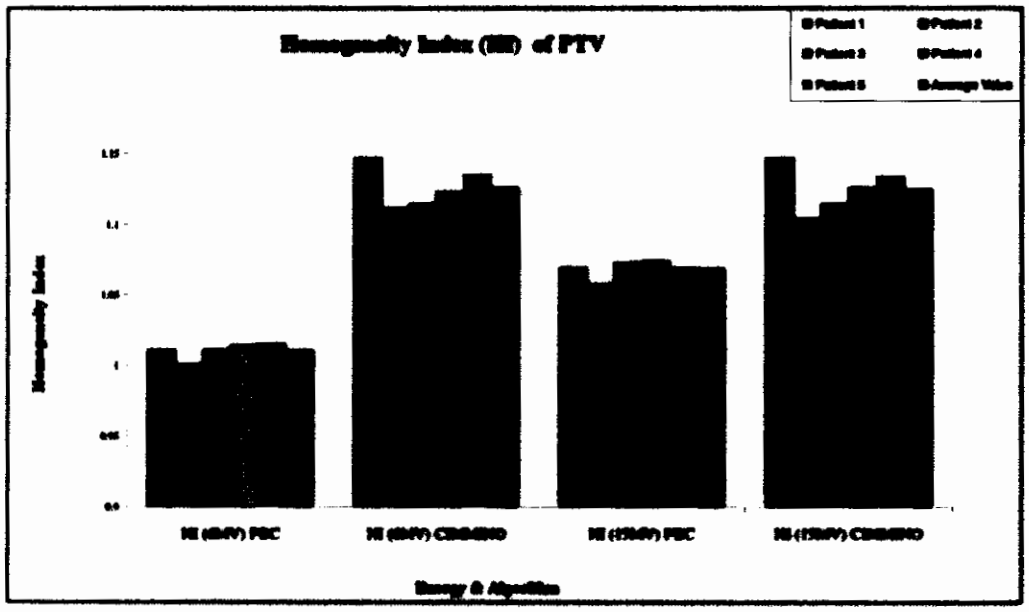

Figure (6.7) Homogeneity Index of PTV for PBC and CIMMINO algorithm with respect to 6MV and 15 MV photon energies.

Normal Lung (P-Lung)

Normal lung (P-lung) significantly getting low dose in those treatment plans which were optimized with CIMMINO algorithm than the PBC algorithm for both energies.

Patient (1)

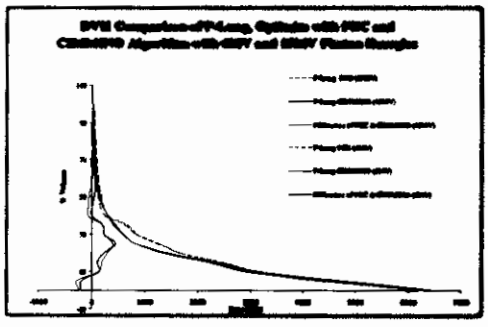

Patient (2)

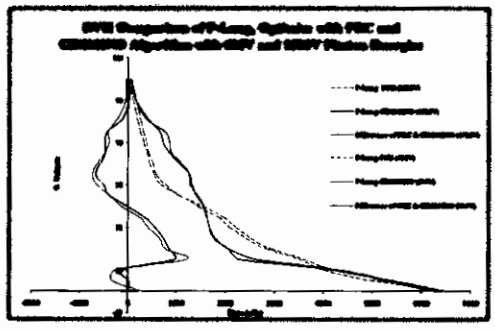

Patient (3)

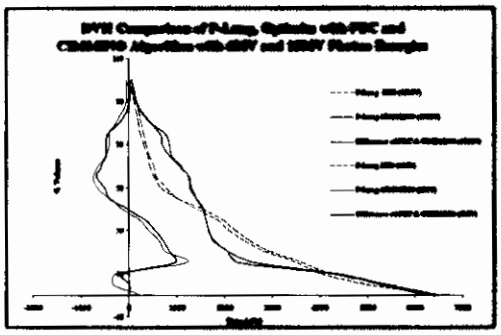

Patient (4)

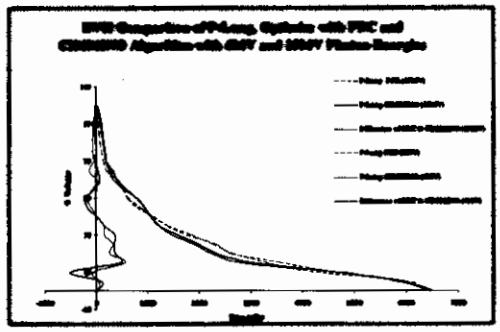

Patient (5)

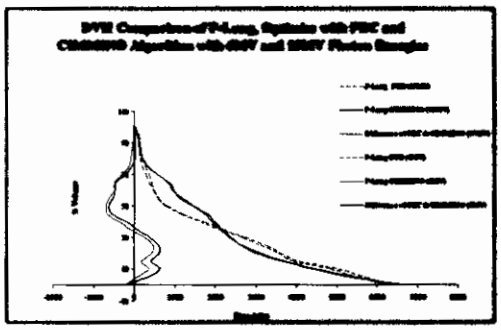

Figure (6.8) Dose Volume Histogram (DVH) and dose difference comparison of Normal Lungs (P-Lung) between PBC and CIMMINO algorithm for 6MV and 15 MV photon energies treatment plans.

In patients (1) and (3) the difference of dose was not significantly high except from 40% to 20% volume of P-Lung for both the energies. In remaining three patients significant dose variation had seen for both energies. But in patient (2) and (4) the P-lung dose increases from 100% to 40% volume and decrease from 40% to 0 volumes in those treatment plans which were optimize with CIMMINO algorithm for both energies. But in patient (5) P-Lung getting significant high dose in those treatment plans which were optimized with the PBC algorithm for both the energies. But overall, it can be concluded that the mean dose of P-Lung volume is high in those treatment plans which were optimized with the PBC algorithm than the CIMMINO for both energies as shown in figure (6.8). But DVH difference in P-Lung volume was little bit higher in the 15MV treatment plans than the 6MV as shown in the figure (6.8) but overall trend of the dose

difference was same. It was seem that the PBC algorithm was overestimating the dose in the lung region than the CIMMINO algorithm. Those treatment plans which were optimized with the PBC or CIMMINO algorithms were showing slightly different DVH of P-Lung for both the photon energies in all patients.

Esophagus

Similarly the DVH of esophagus was compared for each patient. Overall dose calculated by the PBC algorithm was higher than the CIMMINO algorithm for both the energies as shown in the figure (6.9). But in patient (3) and (4) it had seen that the dose variation was not significant for both the energies either the treatment plans were optimized with PBC or CIMMINO algorithm. It shows that both the algorithm calculated the similar dose with respect to the volume of Esophagus. In patient (2) 30% to 100% volume getting the higher dose in those treatment plans which were optimized with the CIMMINO algorithm but the reaming 30% volume getting the approximately similar dose distribution in PBC and CIMMINO algorithm for both the energies. The calculated DVH difference of esophagus in PBC and CIMMINO algorithm for 6MV and 15MV photon energies treatment plans were almost similar in each patient as shown in the figure (6.9). Those treatment plans which were optimized with the PBC or CIMMINO algorithms are showing slightly different DVH of Esophagus for both the photon energies in all patients.

Patient (1)

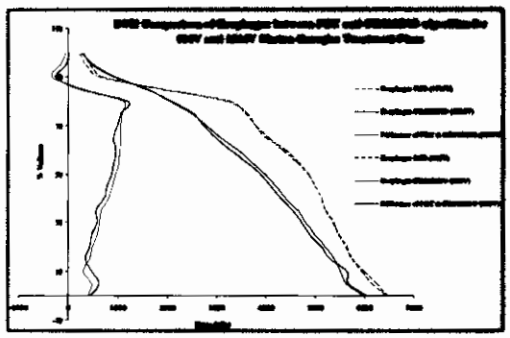

Patient (2)

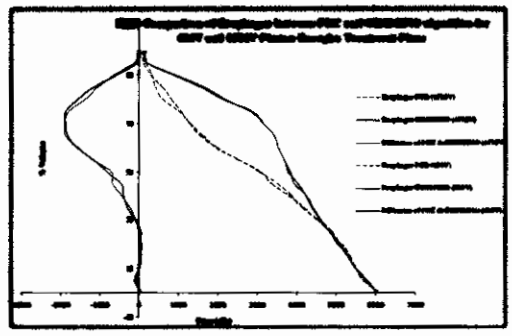

Patient (3)

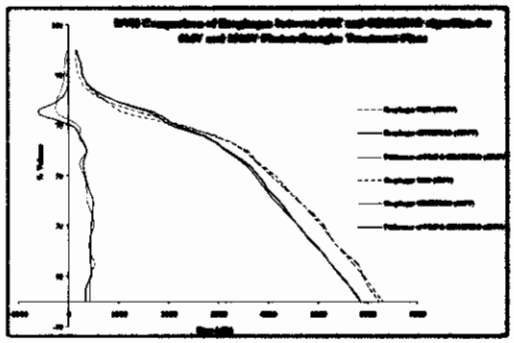

Patient (4)

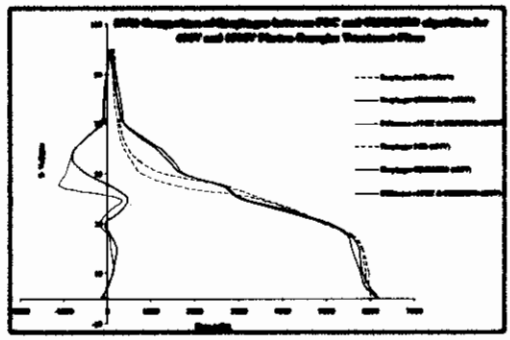

Patient (5)

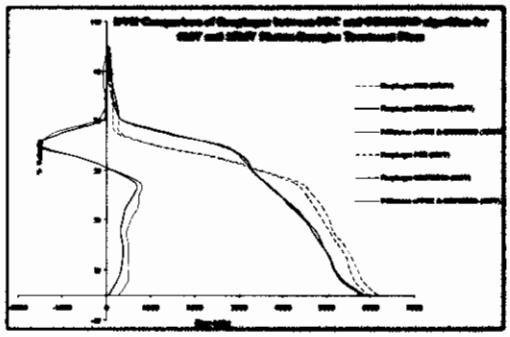

Figure (6.9) DVH and dose difference comparison of Esophagus between PBC and CIMMINO Algorithm for 6MV and 15 MV photon energies treatment plans.

Spinal Cord

DVH comparison of spinal cord was done for all the patients and it was found that the spinal cord dose was higher in those treatment plans which were optimized with the PBC algorithm than the CIMMINO algorithm. This difference was not prominent between 80% to 100% volume of the spinal cord for both the energies in all patients. But in Patient 1 and 2 the DVH difference was very high as compared to the remaining three patients. But overall the dose of the spinal cord was higher in those treatment plans which were optimized with PBC algorithm. DVH comparison of the all the patient with both the energies are shown in the figure (6.10).

Patient (1)

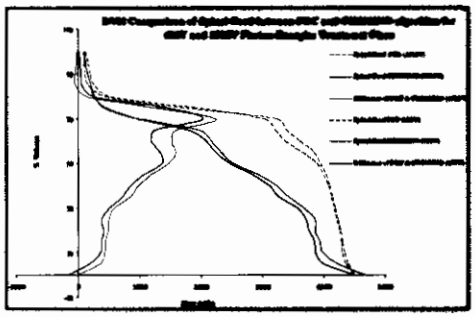

Patient (2)

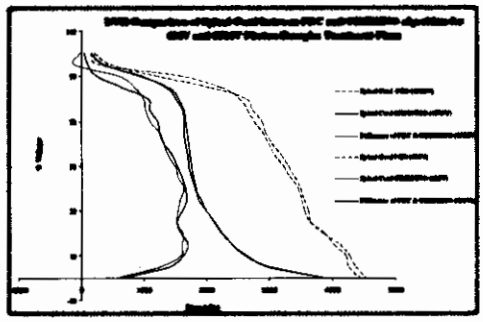

Patient (3)

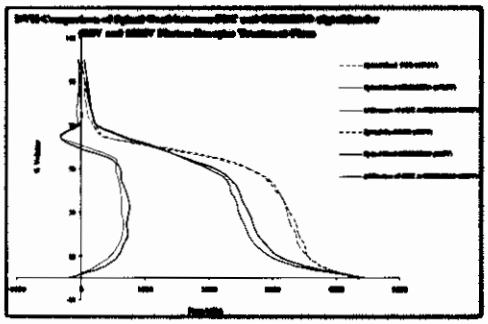

Patient (4)

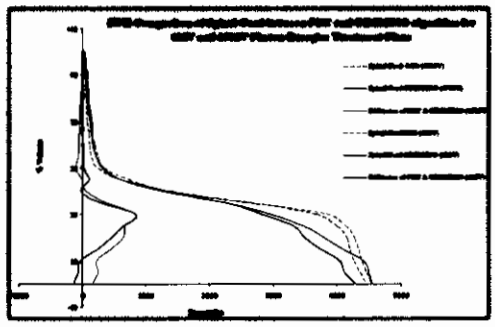

Patient (5)

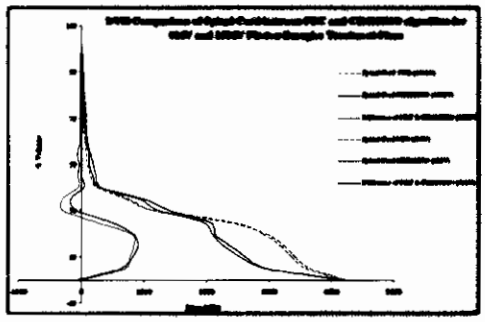

Figure (6.10) DVH and dose difference comparison of Spinal Cord between PBC and CIMMINO Algorithm for 6MV and 15 MV photon energies treatment plans.

Heart

In patient (1) Heart is not included as a ORA's because the tumor was located in the upper left lobe of the lung so that DVH comparison of remaining patients was done in this study. DVH comparison of Heart for PBC and CIMMINO algorithms shows the

significant dose difference with respect to volume for both the energies in patient (2), (4) and (5) as shown in the figure (6.11). In patient (3) this difference is not significant. On the whole, PBC algorithm calculated high dose for Heart volume with respect to the CIMMINO algorithm for each patient. During the comparison of Heart it is also observed that those treatment plans which were optimized with the PBC or CIMMINO algorithms are showing slightly different DVH of Heart for both the photon energies in all patients. But the DVH difference of Heart between PBC and CIMMINO algorithm for different energies is not significant in each patient as shown in the figure (6.11).

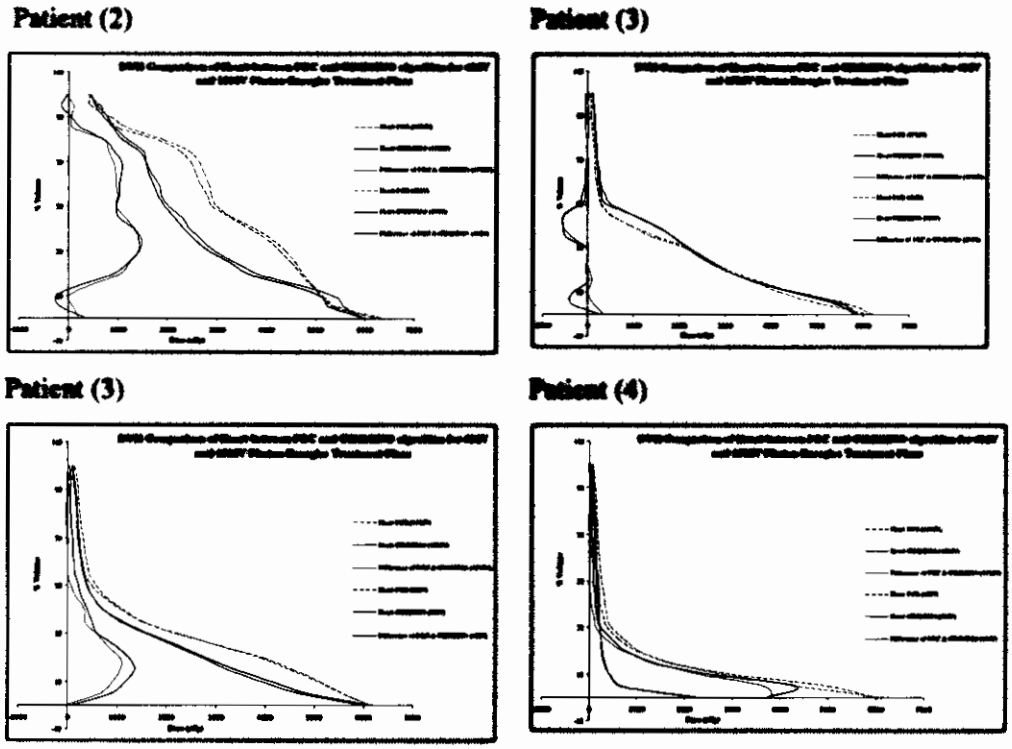

Figure (6.11) DVH and dose difference comparison of Heart between PBC and CIMMINO Algorithm plans for 6MV and 15 MV Photon Energies.

6.4 Small Field Size

6.4.1 Percentage Isodose Comparison

Both treatment planning systems were calibrated at (10×10) cm^2 field size for 100 cGy per 100 MU so this the main reason to compare this field size and try to find the difference of inhomogeneities correction done by the both the treatment planning systems and try to investigate the difference between the dose calculation between these two planning systems in the lungs region. Treatment plans were evaluated which were generated with 6MV photon energy for (10×10) cm^2 field size on PrecisePLAN and Eclipse treatment planning system. The central axis CT slices of both the treatment plans are shown in the figure (6.12). During the analysis, it had been observed that the same percentage isodose lines in the lung region lying at different depths. It means both the planning systems are calculating the different dose deposition in the lung region. During the comparison it was also observed that the percentage isodose lines spreading perpendicular to the incident of the radiation field in each central axis slice but more dominant in Sagittal slice. It was also found that the hotspot varies from 1% to 3% but overall hotspot is higher in that treatment plans which was optimized with PBC algorithm. And similar behavior was seen during the comparison for 15MV photon energy. But hotspot varies from 1% to 3% higher in that plan which was optimized with the CIMMINO algorithm for 15MV photon energy. The isodose were look like a wedge shaped in that treatment plan which was optimized with the PBC algorithm. But in isodose lines were looked approximately straight in that treatment plan which was optimized with the CIMMINO algorithm. This titled in the isodose curves might be due to that the PBC algorithm did not properly take the body curvature into account and did not correct the calculation due to inhomogeneity effect. Secondly, the absorbed dose at different depth was different in both the treatment plans which were optimized with PBC and CIMMINO algorithm. This effect was more prominent in the 15MV treatment plans which are shown in the figure (6.13).

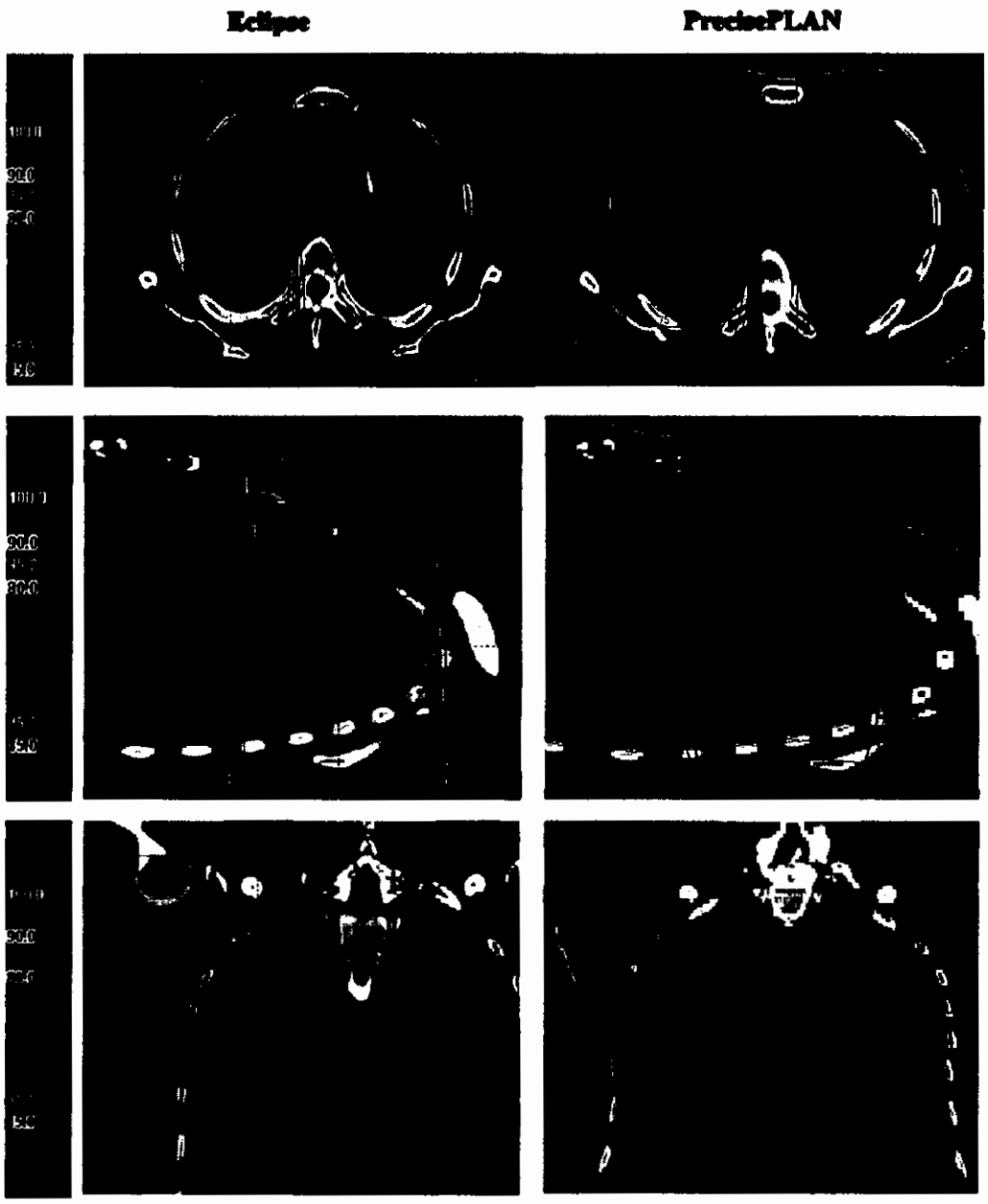

Figure (6.12) Percentage isodose comparisons in Transverse, Sagittal and Coronal Slices for (10×10) cm^2 field size for 6MV photon energy between Eclipse and PreciesPLAN treatment planning system.

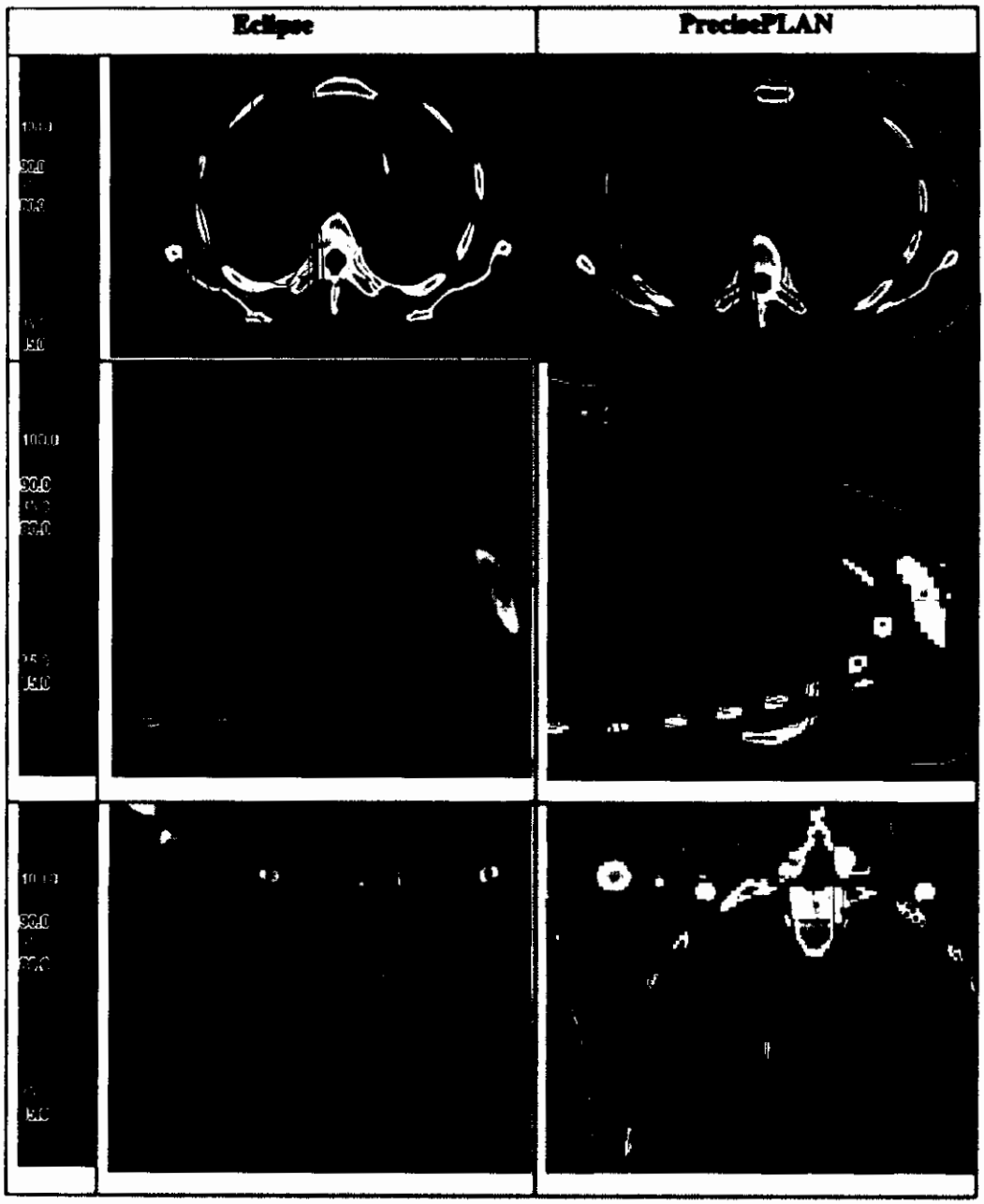

Figure (6.13) Percentage Isodose comparisons in Transverse, Sagittal and Coronal Slices for (10×10) cm^2 field size for 15MV photon energy between Eclipse and PrecisePLAN treatment planning system.

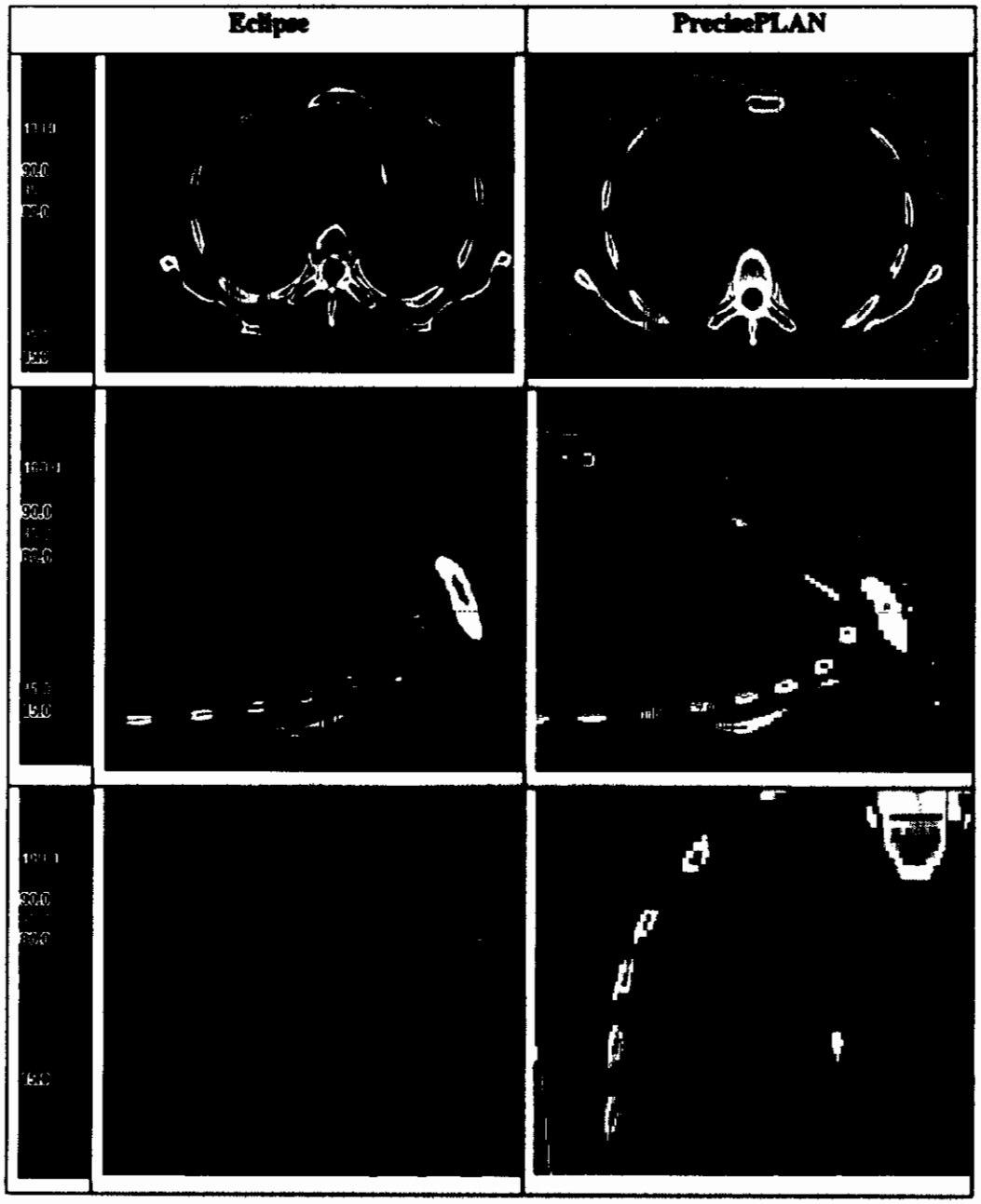

Figure (6.14) Percentage Isodose comparisons in Transverse, Sagittal and Coronal Slices for (2.5×2.5) cm^2 field size for 6MV photon energy between Eclipse and PreciePLAN treatment planning system.

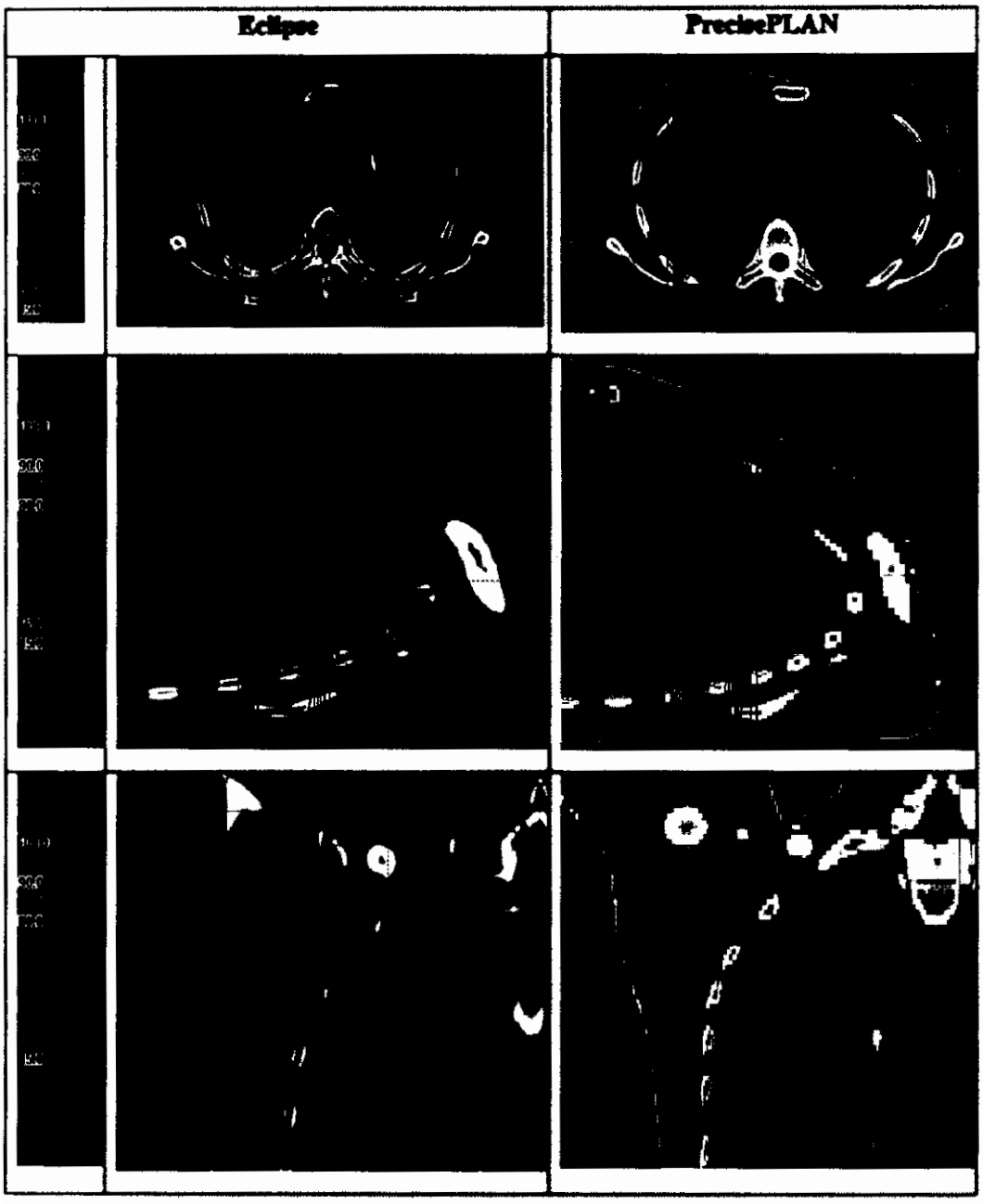

Figure (6.15) Percentage Isodose comparisons in Transverse, Sagittal and Coronal Slices for (2.5×2.5) cm^2 field size for 15MV photon energy between Eclipse and PrecisePLAN treatment planning system.

Similarly we compared percentage Isodose distribution for small field size (2.5×2.5) cm^2 for both the photon energies (6M and 15MV). It was seen that lateral distribution was more significant in that treatment plan which were optimized with the CIMMINO algorithms than the PBC algorithm but this effect was more dominant in Sagittal and Transverse slices for both the energies. Similar behavior was observed for hotspot as we have seen during the comparison of the 6MV and 15MV for (10×10) cm^2 field size. Comparison of the percentage Isodose of both the energies and planning system are shown in the figure (6.14) and (6.15).

6.4.2 Comparison of Minimum, Maximum and Mean Doses (D_{min}, D_{max}, and D_{mean})

Minimum, Maximum and Mean doses (D_{min}, D_{max}, and D_{mean}) in lung were compared for (10×10) cm^2, (2.5×2.5) cm^2 and (3×3) cm^2 field sizes between Eclipse and PreciscPLAN for both the energies as shown in the figure (6.16). For (10×10) cm^2 field size it was found that the D_{min} for both the energies was zero which was planned in Eclipse and PrecisePLAN but D_{max} was slightly high which was planned in Eclipse treatment planning system for both the energies. D_{mean} was significantly low in those plans which were optimized in Eclipse treatment planning system for both energies.

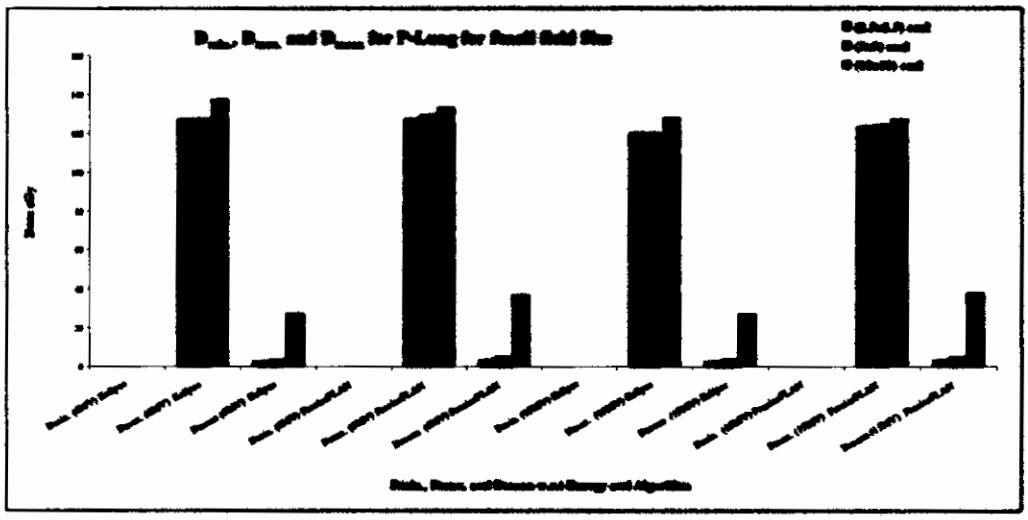

Figure (6.16) Comparison of Minimum, Maximum and Mean Doses (D_{min}, D_{max}, and D_{mean}) of normal lungs (P-Lung) calculated in Eclipse and PreciscPLAN treatment planning systems for 6MV and 15MV photon energies.

Similarly, the $D_{min.}$, D_{mean}, and $D_{max.}$ for (2.5×2.5) cm^2 and (3×3) cm^2 field sizes were evaluation and found that the $D_{min.}$ for both the energies is zero in Eclipse and PrecisePLAN treatment planning system and $D_{max.}$ was almost similar for 6MV and for 15MV plans. Maximum dose ($D_{max.}$) was slightly high in those plans which were optimized in PrecisePLAN treatment planning system. D_{mean} was showing the no significant difference for both energies.

6.4.3 Comparison of Dose Volume Histogram (DVH) of Normal Lung (P-Lung)

DVH differences was also plotted of P-Lung in DVH for those plans which were planed with the same energies but different planning systems and Eclipse was taken as a reference to calculate this DVH difference. This comparison was done due to study to evaluate the inhomogeneity correction method incorporated by both the treatment planning systems and tried to investigated if there exist any difference between dose calculation in low density region specially lung for the treatment planning systems.

The comparison of the P-lung was done for (10×10) cm^2, (2.5×2.5) cm^2 and (3×3) cm^2 field sizes between the dose calculation algorithms of Eclipse and PrecisePLAN treatment planning system for both the photon energies. Significant difference had been seen in DVH for (10×10) cm^2 field size. This difference was significant from 40% to 25% volume of the P-lung for both the energies. But DVH difference in P-lung volume was higher little bit in the 15MV treatment plans than the 6MV as shown in the figure (6.17). Overall trend of the dose difference with respect to the volume was almost similar. If DVH of P-lung were compared for 6MV and 15MV photon energies plans which were generated in Eclipse it could be seen that the DVHs were not much different for both the energies and similar observations were seen in those treatment plans which were generated in PrecisePLAN treatment planning system.

Similarly, the DVH of P-lung was compared for (2.5×2.5) cm^2 and (3×3) cm^2 field size between the planning systems with respect to energies. The DVH were almost similar and the difference was not significant from 100% to 5% volume of the P-lung between the treatment planning systems for both the field sizes. But for less then 5% volume of the P-

Lung the DVH difference could be seen significant. Maximum diffidence was observed at 2.5% volume of P-lung. This difference was negative for 6MVwhilhc implying that the DVH calculated by PrecisePLAN was higher than the Eclipse treatment planning system.

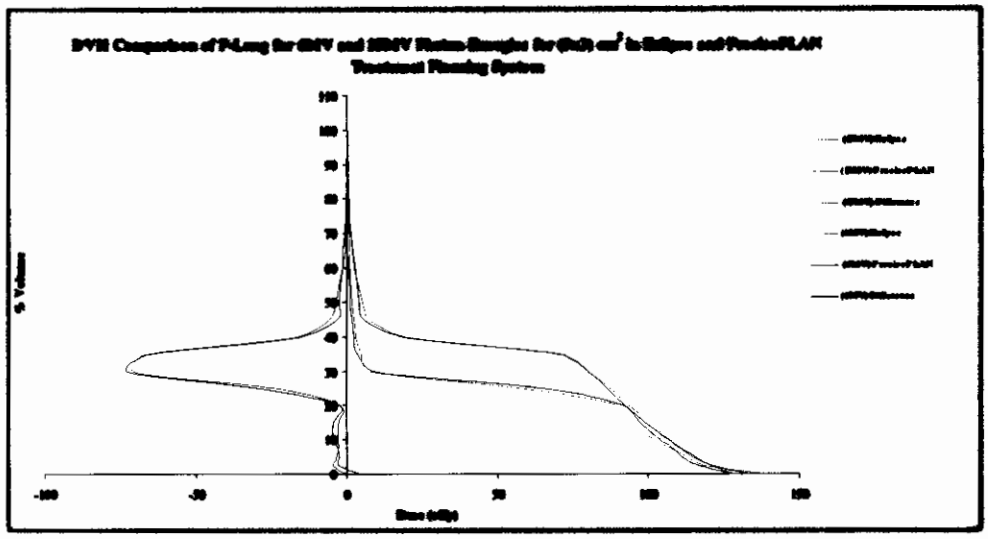

Figure (6.17) DVH and dose difference comparison of (10×10) cm^2 field size for P-Lung between Eclipse and PrecisePLAN treatment planning systems for 6MV and 15 MV Photon Energies.

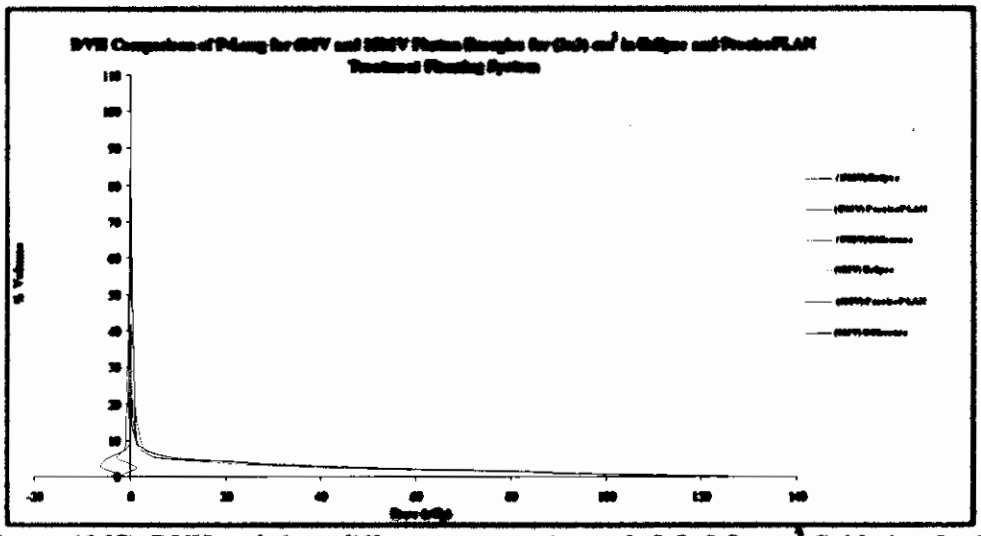

Figure (6.18) DVH and dose difference comparison of (2.5×2.5) cm^2 field size for P-Lung between Eclipse and PrecisePLAN treatment planning systems for 6MV and 15 MV Photon Energies.

However, for 15MV, similar behavior of dose at this volume of P-Lung was seen, as shown in figure (6.18) and (6.19) but this difference is lesser than the 6MV. In the light of these results, it can be said that both the planning systems are calculating the similar dose distribution in the lung region for low (6MV) and high (15MV) energies.

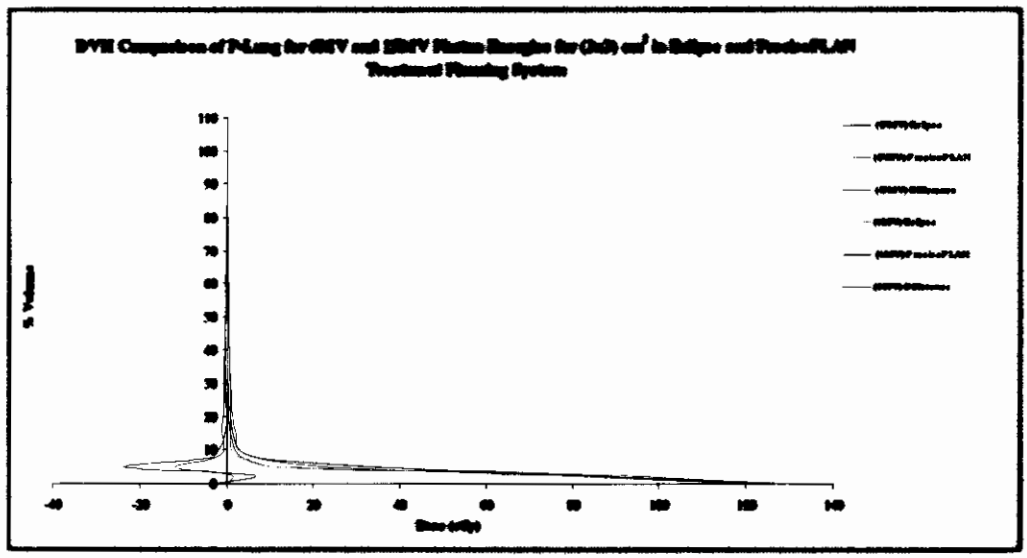

Figure (6.19) DVH and dose difference comparison of (3x3) cm^2 field size for P-Lung between Eclipse and PrecisePLAN treatment planning systems for 6MV and 15 MV Photon Energies.

6.5 Discussion

The accuracy in the dose diffused at a point in the patient is due to a self-governing sources of errors together with patient movement, day to day variation in machine output, of dose calibration of machine, uncertainties in complex calculation, irregular patient contour and the inhomogeneities in the body.

In recent research work, it was observe that the hndose distributions in the low density area may be over estimating by the PBC algorithm for both the photon energies because in PBC algorithm, dose at an arbitrary point located between the standard planes is interpolated along the fanlines of beam [136] and secondly, it does not consider the secondary electron lateral scatter outside the radiation beam that may be the reason to

overestimating the dose in Contralateral lung. But the CIMMINO algorithm estimated the tissues inhomogeneities in different way and presenting the low dose in the Contralateral lung. It may be because the primary component is computed in CIMMINO algorithm and includes the transmission through patient inhomogeneities as well. The CIMMINO algorithm is computed the scatter component and includes the presence of blocks, beam compensators, and curvature of the patient, but not patient inhomogeneities [137, 138].

Hotspot was low in those treatment plans which were optimized with the PBC algorithm for both the energies. It may because the sliding window treatment planning technique was used to generate the treatment plans. However, sliding window technique provides higher degree of freedom to generate the unlimited apertures due to continuous motion of the MLCs to modulate the dose according to the user defined dose constrains to the target and OARs. However, aperture base IMRT technique was used to optimize the treatment plans with CIMMINO algorithm and aperture base IMRT offers to create the limited number of apertures; due to this reason the radiation beam modulation has limited as compared to the sliding window technique. This may be the cause of higher hotspot in those treatment plans which were optimized by CIMMINO algorithm for both energies. Dmin., Dmax. and Dmean values for each OARs were different for each photon energy in each patient for each dose calculation algorithms. Mean doses of five patients calculated with both algorithms for PTV, P-Lung and Esophagus, is almost similar for both the photon energies. It may be because each algorithm is calculating the different weighted radiation beam configuration for 6MV and 15MV photon energy to fulfill the prescribed dose limits to and target and tolerance dose limits of OARs. Mean dose of the Heart and Spinal Cord was high in the 6MV treatment plans than the 15MV. Because 15MV photon energy has low energy deposit rate than 6MV and both the algorithms calculated according to the beam quality of the photon energy.

DVH of PTV was steeped in PBC algorithm than the CIMMINO algorithm for both the energies because PBC algorithm was overestimating the dose inhomogeneities correction and secondly the sliding window technique provides the better solutions to fulfill the user defined dose constrains. But overall the dose distribution of the PTV in all patients was

little bit better in those treatment plans which were optimized with the CIMMNIO algorithms. This result shows that both the algorithms provide the reasonable dose coverage of PTV but slightly different minimum and maximum dose.

In general, for any lung tumor the dose is calculated with suitable precision at the ICRU reference point. Due to the assumption of electron and photon equilibrium the accuracy of the algorithms is inadequate. At the center of a unit density gross tumor volume offers approximately entire electron and photon equilibrium at the ICRU reference point location, hence the comparatively small inaccuracy predicts at this position. These situations illustrate the high precision with which the dose could be computed even with unsophisticated algorithms [139] at the ICRU reference point. The electron transport in the lung may cause the differences dose, which is not effectively computed by the unsophisticated algorithms. Clinically unacceptable inaccuracies will be introduced for high photon energies due to the variety of small field engaged for IMRT, leading to under dosage or overdose the target. Unsophisticated algorithms can miscalculate in the lung boundaries regions that due to one Dimension (1D) inhomogeneity correction may be misleading in clinically environment.

DVH comparison of P-lung showed that the PBC algorithm was overestimating and presenting the significant DVH difference with respect to the CIMMINO algorithm for both the energies. It may be the reason that CIMMINO algorithm is not computed the patient inhomogeneities for scatter component of the primary radiation beam. Each algorithm was calculating similar DVH for P-Lung for both the photon energies because the different weighted radiation beam configuration was arrange during the optimization for 6MV and 15MV photon energy to fulfill user defined dose constrains of OARs and target dose coverage. Similar behavior was seen for other OARs like Heart, Esophagus and Spinal Cord. DVH of Spinal Cord was significantly different form 80% volume to 5% volume between PBC and CIMMINO algorithm treatment plans but maximum dose (45Gy) of the Spinal Cord does not exceed in both the algorithms. It means that the CIMMINO algorithm modulates the radiation beams in better way than the PBC

algorithm to deliver the same amount of the dose with delivering the low dose to the spinal cord.

Inhomogeneity correction between the both the treatment planning systems were also investigated for both the photon energies. Percentage Isodose distribution was significantly different for (10×10) cm^2 field size between PrecisePLAN and Eclipse treatment planning system in lung region for both the energies. That shows each planning system handle inhomogeneities in different way and different estimation in dose calculated was undertaken by each treatment planning system due to differently handling the primary and secondary components of the radiation beam. PrecisePLAN uses the Equivalent Slant Depth algorithm for inhomogeneities correction. Numbers of publications warn the unsophisticated algorithms in inaccurate dose prediction inside or in the vicinity of lung medium. These algorithms are used regularly in hand calculation and computerized TPS, but primarily have been authorizing for cobalt-60 radiotherapy. In the regions of electron disequilibrium, the ordinary correction base algorithms do not compute the dose accurately, like lung and target boundaries and near the ends of a field. The dose calculation accuracy affect significantly for high energies (>10 MV) and it is particularly essential for three dimensional (3D) dose calculation TPSs. A lot of publications evidently have established the failure of equivalent path length based algorithms in lung radiotherapy [139, 143].

Eclipse uses the Modified Batho Power Law algorithm for inhomogeneities correction. The above mentioned inhomogeneity correction models were formulated during that period when photon energies tended to be low energy range like cobalt-60, 4MV, and 6MV x-ray energies. The estimation of electron equilibrium was satisfactory and thus tissue air ratio information could be considered to adjust directly. These methods cannot be expanded for electron non-equilibrium conditions [144, 145].

Small field (2.5×2.5) cm^2 and (3×3) cm^2 were investigated in this study and significant difference was observed in isodsose distribution and dose in the penumbra region. This effect is similar as seen for (10×10) cm^2 field size. Dose in penumbra region was different due the low density regions and secondary scatter. This effect occur because

electron energy is scattered outside the field is higher than the scattered towards the central axis due to the small field aperture. The beam energy strongly influenced in this effect and the tissues the density contributed at lower extent for the finite aperture size. Due to this phenomenon the beam boundaries are distorted in low density region, because the lateral motion of charged particles is increased. Several authors explained the dispersion of secondary electrons from high energy beams [57, 59], [146]. The impression of primary and scatter components could be expended in non-equilibrium conditions.

From above discussion it is concluded that the inhomogeneity correction is more complicated in IMRT, than for 3DCRT. Whereas, the Batho Power Law algorithm is limited, due to the limitation of lateral charged particle equilibrium. Dose inaccuracies in the computed depth dose occur due to ignore the electron transport [67]. The error in dose computation is directly proportional to the field size and inversely proportional to the density of the inhomogeneity and high photon energies (> 10 MV) [147, 148].

Chapter (07)

CONCLUSIONS

In this study, Pencil Beam Convolution (Eclipse TPS) and CIMMINO algorithm (PrecisePLAN TPS) are compared using IMRT technique for 6MV and 15MV photon energies for non-small cell lung cancer (NSCLC) case. Within the target structures the deviations of hotspot, mean dose, percentage Isodose distribution and DVH variation between the algorithms were recorded. Variation between algorithms was recorded for PTV, Lung, Esophagus, Spinal Cord and Heart doses. Analyses were performed by comparison the Percentage Isodose distribution, hotspot, mean dose and DVH and its differences with prescribed dose, Homogeneity Index for target structures for 6MV and 15MV photon energies. CIMMINO algorithm showed better results than the PBC algorithms in term of PTV dose coverage, and dose to OAR's. Lung Inhomogeneity correction of PrecisePLAN and Eclipse treatment planning system for 6MV and 15MV photon energies was accessed for (10×10) cm^2 and small field sizes (2.5×2.5) cm^2 and (3×3) cm^2. Percentage Isodose distribution, minimum doses, maximum doses and mean doses, DVH of Lung was compared to analyze the inhomogeneity correction difference for these three field sizes. Significant difference was observed in percentage Isodose distribution, hotspot, mean doses between the Eclipse and PrecisePLAN treatment planning system. In this study as the results differed from each other significantly, extensive precautions should be consider during the evaluation of treatment plans, as the option of the dose computation algorithm may manipulate the treatment plans in addition to clinical outcome.

REFERENCES

1- IAEA Commissioning and quality assurance of computerized planning systems for radiation treatment of cancer *TRS-430* (Vienna: IAEA) (2005).

2- AAPM Report 85 Tissue inhomogeneity corrections for MV photon beams *Report of Task Group No. 65 of the Radiation therapy Committee of the American Association of Physicists in Medicine* (Madison, WI: Medical Physics Publishing) (2004).

3- Cheng C W, Das I J, Tang W, Chang S, Tsai J S, Ceberg C, De Gaspie B, Singh R, Fein D A and Fowble B "Dosimetric comparison of treatment planning systems in irradiation of breast with tangential fields" *Int. J. Radiat.Oncol. Biol. Phys.* **38** 835–42 (1997).s

4- ICRU Report 44 *Tissue Substitutes in Radiation Dosimetry and Measurement* (Oxford: Oxford University Press) IEC62083 2000 *Medical Electrical Equipment—Requirements for the Safety of Radiotherapy Treatment Planning Systems* 1st edn (IEC62083) (Geneva: IEC) (1989).

5- Mijnheer B, Olszewska A, Fiorino C, Hartmann G, Kn¨o¨os T, Rosenwald J C and Welleweerd H 2004 (Brussels:ESTRO).

6- Clarkson J R "A note on depth doses in fields of irregular shape" *Br. J. Radiol.* **14** 255 Cunningham J R 1972 Scatter–air ratios *Phys. Med. Biol.* **17** 42–51 (1944).

7- Cunningham J R, Shrivastava P N and Wilkinson J M Program IRREG-calculation of dose from irregularly shaped radiation beams *Comput. Programs Biomed.* **2** 192–9 (1972).

8- O'Connor J, "The variation for scattered x-rays with density in an irradiated body," *Phys. Med. Biol.* **1** 352–69 (1957)

9- Sontag M R and Cunningham J R, "Clinical application of a CT based treatment planning system," *Comput.Tomogr.* **2** 117–30 (1978a)

10- Sontag MR and Cunningham J R "The equivalent tissue–air ratio method formaking absorbed dose calculations in a heterogeneous medium" *Radiology* **129** 787–94 (1978).

11- Aspradakis M M, Morrison R H, Richmond N D and Steele A "Experimental verification of convolution/ superposition photon dose calculations for radiotherapy treatment planning" *Phys. Med. Biol.* **48** 2873–93 (2003).

12- Woo M and Cunningham J "The validity of the density scaling method in primary electron transport for photon and electron beams" *Med. Phys.* **17** 187–94 (1990).

13- Keall P and Hoban P "Accounting for primary electron scatter in x-ray beam convolution calculations" *Med. Phys.* **22** 1413–8 (1995).

14- Keall P J and Hoban P W "Superposition dose calculation incorporating Monte Carlo generated electron track kernels" *Med. Phys.* **23** 479–85 (1996).

15- Miften M, Wiesmeyer M, Kapur A and Ma C M "Comparison of RTP dose distributions in heterogeneous phantoms with the BEAM Monte Carlo simulation system" *J. Appl. Clin. Med. Phys.* **2** 21–31 (2001).

16- Ahnesj¨o A, Weber L, Murman A, Saxner M, Thorslund I and Traneus E "Beam modeling and verification of a photon beam multisource model" *Med. Phys.* **32** 1722–37 (2005).

17- "Radiation Treatment Planning Dosimetry Verification," A APM Radiation Therapy Committee Task Group #23 (1995).

18- VAN DYK, J., BARNETT, R.B., BATTISTA, J.J., "Computerized radiation treatment planning systems", The Modern Technology of Radiation Oncology: A Compendium for Medical Physicists and Radiation Oncologists (VAN DYK, J., Ed.), Medical Physics Publishing, Madison, WI Ch. 8 (1999).

19- International Commission on Radiation Units and Measurements, Use of Computers in External Beam Radiotherapy Procedures with High-energy Photons and Electrons, Rep. 42, ICRU, Bethesda, MD (1987).

20- AHNESJÖ, A., ASPRADAKIS, M.M., Dose calculations for external photon beams in radiotherapy, Phys. Med. Biol. **44** R99–R155 (1999).

21- Behrens C F "Dose build-up behind air cavities for Co–60, 4, 6 and 8 MV. Measurements and Monte Carlo simulations" *Phys. Med. Biol.* **51** 5937–50 (2006).

22- Klein E E, Chin L M, Rice R K and Mijnheer B J "The influence of air cavities on interface doses for photon beans" *Int. J. Radiat. Oncol. Biol. Phys.* **27** 419–27 (1993).

23- Krieger T and Sauer O A "Monte Carlo- versus pencil-beam-/collapsed-cone-dose calculation in a heterogeneous multi-layer phantom" *Phys. Med. Biol.* **50** 859–68 (2005).

24- Tsiakalos M F, Stathakis S, Plataniotis G A, Kappas C and Theodorou K "Monte Carlo dosimetric evaluation of high energy vs low energy photon beams in low density tissues" *Radiother. Oncol.* **79** 131–8 (2006).

25- Vanderstraeten B, Reynaert N, Paelinck L, Madani I, Wagter C D, Gersem W D, Neve W D and Thierens H "Accuracy of patient dose calculation for lung IMRT: a comparison of Monte Carlo, convolution/superposition, and pencil beam computations" *Med. Phys.* **33** 3149–58 (2006).

26- R. Mohan, "Monte Carlo Simulation of Radiation Treatment Machine Heads," in *Monte Carlo Transport of Electrons and Photons*," T. M. Jenkins, W. R. Nelson, A. Rindi (eds.), (New York: Plenum Press), pp. 453–468 (1988).

27- D. W. O. Rogers, B. A. Faddegon, G. X. Ding, C.-M. Ma, J. We, and T. R. Mackie, "BEAM - A Monte Carlo code to simulate radiotherapy treatment units," *Med. Phys.* 22:503–524 (1995).

28- F. A. Attix, *Introduction to Radiological Physics and Radiation Dosimetry*, (New York: Wiley) (1986).

29- H. E. Johns and J. R. Cunningham, *The Physics of Radiology*, (Springfield, IL: C.C. Thomas) (1983).

30- D. W. O. Rogers, "Fluence to dose equivalent conversion factors calculated with EGS3 for electrons from 100 keV to 20 GeV and photons from 11 keV to 20 GeV," *Health Phys.* 46:891–914 (1984).

31- A. Ahnesjo, P. Andreo, and A. Brahme, "Calculation and application of point spread functions for treatment planning with high energy photon beams", *Acta Oncologica* 26:49–56 (1987).

32- N. Papanikolaou and T. R. Mackie, "Extension of the convolution/superposition based algorithms to include atomic number effects," *Med. Phys.* 22:977 (1995).

33- R. Alecu, C. Reft, I. J. Das, B. J. Gerbi, P. Keall, E. Lief, B. J. Mijnheer, N. Papanikolaou, C. Sibata, and J. Van Dyk, "Dosimetric considerations for patients with hip prostheses undergoing pelvic irradiation," Report of the AAPM Radiation Therapy Committee Task Group 63, *Med. Phys.* 30(6):1162–1182 (2003).

34- J. McLellan, L. Papiez, G. A. Sandison, W. Huda, and P. Therrien, "A numerical method for electron transport calculations", *Phys. Med. Biol.* 37:1109–25 (1992).

35- G. Starkschall, A. A. Shiu, S. W. Bujnowski, L. L. Wang, D. A. Low, and K. R. Hogstrom, "Effect of dimensionality of heterogeneity corrections on the implementation of a three-dimensional electron pencil-beam algorithm," *Phys. Med. Biol.* 36(2):207–227 (1991).

36- I. Kawrakow, M. Fippel, and K. Friedrich, "3D electron dose calculation using a voxel based monte carlo algorithm," *Med. Phys.* 23:445–457 (1996).

37- I. Kawrakow, "Accurate condensed history Monte Carlo simulation of electron transport. I. EGSnrc, the new EGS4 version," *Med. Phys.* 27:485–98 (2000).

38- M. K. Woo, D. Scora, and E. Webb, "The regional Monte Carlo method: a dose calculation method based on accuracy requirement," *Med. Phys.* 25:1866–1871 (1998).

39- I. Kawrakow, "Accurate condensed history Monte Carlo simulation of electron transport. II. Application to ion chamber response simulations," *Med. Phys.*27:499–513 (2000).

40- I. Kawrakow, "VMC++, Electron and Photon Monte Carlo Calculations Optimized for Radiation Treatment Planning," in *Advanced Monte Carlo for Radiation Physics, Particle Transport Simulation and Applications: Proc. Monte Carlo 2000 Meeting* Lisbon, A. Kling, F. Barao, M. Nakagawa, L. Tavora, and P. Vaz (eds.), (Berlin: Springer), pp. 229–236 (2001).

41- H. Neuenschwander, T. R. Mackie, and P. Reckwerdt, "MMC-a high-performance Monte Carlo code for electron beam treatment planning," *Phys. Med. Biol.* 40(4):543–74 (1995).

42- M. Fippel, I. Kawrakow, K. Friedrich, "Electron beam dose calculations with the VMC algorithm and the verification data of the NCI working group," *Phys. Med. Biol.* 42:501–20 (1997).

43- C. Manfredotti, U. Nastasi, R. Marchisio, C. Ongaro, G. Gervino, R. Ragona, S. Anglesio and G. Sannazzari, "Monte Carlo simulation of dose distribution in electron beam radiotherapy treatment planning," *Nucl. Instrum. Methods* A291:646–54 (1990).

44- P. Keall and P. Hoban, "A review of electron beam dose calculation algorithms," *Australas. Phys. Eng. Sci. Med.* 19:111–30 (1996).

45- G. A. Carlsson, "Absorbed dose equations. on the derivation of a general absorbed dose equation and equations valid for different kinds, of radiation equilibrium," *Radiat. Res.* 85:219–237 (1981).

46- A. Dutreix and A. Bridier, "Dosimetry for External Beams of Photon and Electron Radiation" (Chapter 3) in *The Dosimetry of Ionizing Radiation,*" Kenneth R. Kase, Bengt Björngard, and Frank Attix (eds.), (San Diego: Academic Press Inc., Harcourt Brace Jovanovitch) V.1, pp. 163–228 (1985).

47- A. A. Mustafa and D. F. Jackson, "The relationship between x-ray CT numbers and charged particle stopping powers and its significance in radiotherapy treatment planning," *Phys. Med. Biol.* 28:169–76 (1983).

48- E. C. McCullough and A. M. Krueger, "Performance evaluation of computerized treatment planning systems for radiotherapy: external photon beams," *Int. J. Radiat. Oncol. Biol. Phys.* 6:1599–1605 (1980).

49- R. Mohan, C. S. Chui, and L. Lidofsky "Differential pencil beam dose computational model for photons," *Med. Phy. 13:64-73* (1986).

50- J. J. Battista, M. J. Bronskill, "Compton scatter imaging of transverse sections: an overall appraisal and evaluation for radiotherapy planning," *Phys. Med. Biol.* 26:81–99 (1981).

51- J. E. O'Connor, "The variation of scattered x-rays with density in an irradiated body," *Phys. Med. Biol.* 1:352–69 (1957).

52- U. Fano, "Note on the Bragg-Gray cavity principle for measuring energy dissipation," *Radiat. Res.* 1:237–40 (1954).

53- P. J. Gullane, "Primary mandibular reconstruction: analysis of 64 cases and evaluation of interface radiation dosimetry on bridging plates," *Laryngoscope* 101:1–24 (1991).

54- D. Harder, "Fano's theorem and the multiple scattering correction," *Fourth Symposium On Microdosimetry* (Verbania –Pallanza, Italy) J. Booz, H. G. Ebert, R. Eickel, and A. Waker (eds.) (Luxembourg: Commission of the European Communities), pp. 677–93 (1974).

55- B. E. Bjarngard, "On Fano's and O'Connor's theorems," *Radiat. Res.* 109:184–9 (1987).

56- M. B. Sharpe, A Unified Approach of Calculating the Dose Rate and Dose Distribution for Therapeutic X-Ray Beams," Ph.D. Thesis. University of Western Ontario, London, ON Canada.

57- K. E. Ekstrand and W. H. Barnes, "Pitfalls in the use of high energy x-rays to treat tumors in the lung," *Int. J. Radiat. Oncol. Biol. Phys.* 18:249–252 (1990).

58- ICRU Report No. 50, "Prescribing, Recording and Reporting Photon Beam Therapy," (Washington, DC: International Commission on Radiation Units and measurements) (1994).

59- M. K. Woo, J. R. Cunningham, and J. J. Jeziorenski, "Extending the concept of primary and scatter separation to the condition of electronic disequilibrium," *Med. Phys.* 17:588–595 (1990).

60- A. Dutreix, B. E. Bjarngard, A. Bridier, B. Mijnheer, J. E. Shaw, and H. Svensson, "Monitor Unit Calculation For High Energy Photon Beams," in *Physics for Clinical Radiotherapy Booklet No. 3*, European Society for Therapeutic Radiology and Oncology (ESTRO), ed. Garant Publishers N.V. (1997).

61- J. J. Battista, M. B. Sharpe, "True three-dimensional dose computations for megavoltage x-ray therapy: a role for the superposition principle," *Australas. Phys. Eng. Sci. Med.* 15:159–78 (1992).

62- G. C. Field and J. J. Battista, "Photon Dose Calculations Using Convolution in Real and Fourier Space: Assumptions and Time Estimates," *Proceedings of the 9th International Conference on Computers in Radiation Therapy*, (New York, Elsevier) pp. 103–106 (1987).

63- J. Van Dyke, R. B. Barnett, J. E. Cygler, and P. C. Shragge, "Commissioning and quality assurance of treatment planning computers," *Int. J. Radiat. Oncol., Biol., Phys.* **26**, 261–273 (1992).

64- P. Andreo, "Monte Carlo techniques in medical radiation physics," *Phys. Med. Biol.* **26**, 861–920 (1991).

65- T. R. Mackie, J. W. Scrimger, and J. J. Battista, "A convolution method of calculating dose for 15 MV X-rays,"*Med. Phys.* **12**, 188–196 (1985)

66- R. Mohan, "Why Monte Carlo?," in Proceedings of the XIIth International Conference on the Use of Computers in Radiation Therapy, Salt Lake City, UT, edited by D. D. Leavitt and G. Starkschall ~*Medical Physics Publishing*, Madison, WI, 1997!, pp. 16–18.

67- M. R. Arnfield, C. Hartmann Siantar, J. Siebers, P. Garmon, L. Cox, and R. Mohan, "The impact of electron transport on the accuracy of computed dose," *Med. Phys.* **27**, 1266–1274 (2000).

68- T. R. Mackie, P. Reckwerdt, T. McNutt, M. Gehring, and C. Sanders, "Photon Beam Dose Computations," in T.R. Mackie, J.R. Palta (editors). *Teletherapy: Present and Future.* (Madison, WI:Advanced Medical Publishing) pp. 103–135 (1996).

69- Photon Treatment Planning Collaborative Working Group, M. Goitein, J. Laughlin, J. Purdy, M. R. Sontag, "Evaluation of high energy photon external beam treatment planning: project summary," *Int. J. Radiat. Oncol. Biol. Phys.*21:3–8 (1991).

70- Photon Treatment Planning Collaborative Working Group, M. Goitein, J. Laughlin, J. Purdy, and M. R. Sontag, "Three-dimensional dose calculations for radiation treatment planning," *Int. J. Radiat. Oncol. Biol. Phys.* 21:25–36 (1991).

71- Photon Treatment Planning Collaborative Working Group, M. Goitein, J. Laughlin, J. Purdy, and M. R. Sontag, "Role of inhomogeneity corrections in three-dimensional photon treatment planning," *Int. J. Radiat. Oncol. Biol. Phys.* 21:59–69 (1991).

72- Photon Treatment Planning Collaborative Working Group, M. Goitein, J. Laughlin, J. Purdy, and M. R. Sontag, "The clinical three-dimensional treatment planning studies: A prologue," *Int. J. Radiat. Oncol. Biol. Phys.* 21:165–167 (1991).

73- G. J. Kutcher, Z. Fuks, H. Brenner, A. P. Brown, C. Burman, E. Cheng, L. Coia, K. Krippner, J. M. Manolis, R. Mohan, J. R. Simpson, M. Urie, B. Vikram, and R. Wallace, "Three-dimensional photon treatment planning for carcinoma of the nasopharynx," *Int. J. Radiat. Oncol. Biol. Phys.* 21:169–182 (1991).

74- K. Mah and J. Van Dyk, "On the impact of tissue inhomogeneity corrections in clinical thoracic radiation therapy," *Int. J. Radiat. Oncol. Biol. Phys.* 21:1257–1267 (1991).

75- C. G. Orton, S. Chungbin, E. E. Klein, M. T. Gillin, T. E. Schultheiss, and W. T. Sause, "Study of lung density corrections in a clinical trial (RTOG 88-08)," *Int J. Radiat. Oncol. Biol. Phys.* 41(4):787–794 (1998).

76- A. Van't Riet, H. C. Stam, A. C. A. Mak, and F. H. S. van Slooten, "Implications of lung corrections for dose specification in radiotherapy," *Int. J. Radiat. Oncol. Biol. Phys.* 11:621–625 (1985).

77- W. G. McKenna, K. Yeakel, A. Klink, B. A. Fraass, J. van de Geijn, E. Glatstien, and A. Lichter, "Is correction for lung density in radiotherapy treatment planning necessary?" *Int. J. Radiat. Oncol. Biol. Phys.* 13:273–278 (1987).

78- H. J. van Kleffens and B. J. Mijnheer, "Determination of the Accuracy of the Tissue Inhomogeneity Correction in Some Computer Planning Systems for Megavoltage Photon Beams," in *Proceedings of the 8th International Conference*

on the Use of Computers in Radiation Therapy. Toronto, Canada, (Silver Spring, MD: Computer Society Press IEEE), pp. 45–49 (1984).

79- C. G. Orton, P. M. Mondalek, J. T. Spicka, D. S. Herron, L. I. Andres, "Lung corrections in photon beam treatment planning: are we ready?" *Int. J. Radiat. Oncol. Biol. Phys.* 10(12):2191–9 (1984).

80- JOHNS, H.E., CUNNINGHAM, J.R., The Physics of Radiology, Thomas, Springfield, IL (1983).

81- KHAN, F.M., "The Physics of Radiation Therapy", Lippincott, Williams and Wilkins, Baltimore, MD (2003).

82- KHAN, F.M., POTISH, R.A., "Treatment Planning in Radiation Oncology", Lippincott, Williams and Wilkins, Baltimore, MD (1998).

83- Sebastiaan Breedveld, Pascal R M Storchi, Marleen Keijzer, Arnold W Heemink2 and Ben J M Heijmen1, "A novel approach to multi-criteria inverse planning for IMRT", *Phys. Med. Biol.* 52 6339–6353 (2007).

84- Boyer Al, Mok EC., "A photon dose distribution model employing convolution calculations", *Med Phys.* 12:167-177 (1986).

85- Mohan R, Chui C, Lidofsky L., "Differential pencil beam dose compution model for photons " *Med Phys.* 13:64-73 (1986).

86- Mackie TR, Helen HL, McCullough EC., "Treatment Planning Algorithms", In: Khan FM, Potish RA, eds. Treatment Planning in radiation Oncology, Baltimore: Williams & Wilkins; (1998).

87- Gustafsson A, Lind B K, Svensson R and Brahme A Simultaneous optimization of dynamic multileaf collimation and scanning patterns of compensation filters using a generalized pencil beam algorithm *Med. Phys.* **22** 1141–56 (1995).

88- Langer M, Brown R, Urie M, Stracher M and Shapiro J Large angle optimization for beam weights under dose volume restrictions", *Int. J. Radiat. Oncol. Biol. Phys.* **18** 887–93 (1990).

89- Wang X H, Mohan R, Jackson A, Leibel S A, Fuks Z and Ling C C "Optimization of intensity-modulated 3D conformal treatment plans based on biological indices" Radiother. Oncol. **37** 140–152 (1995).

90- Censor Y, Altschuler M D and Powlis W D "On the use of Cimmino's simultaneous projections method for computing a solution of the inverse problem in radiation therapy treatment planning Inverse Problems", *Appl. Math.Comput.* **4** 607–23 (1988).

91- Starkschall G and Eifel P J "An interactive beam-weight optimization tool for three-dimensional radiotherapy treatment planning", Med. Phys. **19** 155–63 (1992).

92- Ekl¨of A, Ahnesj¨o A and Brahme A "Photon beam energy deposition kernels for inverse radiotherapy planning", Acta Oncol. **29** 447–54 (1989).

93- Niemierko A and Goitein M "The use of variable grid spacing to accelerate dose calculations", *Med. Phys* **16** 357–60 (1989).

94- Jolliffe I T "Principal Component Analysis" (New York: Springer) (1986).

95- Zheng-Ming L and Brahme A "An overview of the transport theory of charged particles", Radiat. Phys. Chem. **41** 673–703 (1993).

96- Bortfeld T, Stein J and Preiser K "Clinically relevant intensity modulation optimization using physical criteria" *Proc. XII Int. Conf. on the Use of Computers in Radiation Therapy (27–30 May, Salt Lake City)* ed D D Leavitt and G Starkschall (Madison, WI: Medical Physics Publishing) pp 1–4 (1997).

97- R. Jeraj, P. J. Keall, and J. V. Siebers, "The effect of dose calculation accuracy on inverse treatment planning," *Phys. Med. Biol.* 47:391–407 (2002).

98- N. Papanikolaou, T. R. Mackie, M. Gehring, and J. Fairbanks, "Clinical implementation of a convolution based algorithm for 3D treatment planning,",*Int. J. Radiat. Oncol. Biol. Phys.* 32:302 (1995).

99- N. Papanikolaou, "Dose calculation algorihtms in the IMRT era," *Radiother. Oncol.* 61 (Suppl. 1):S12 (2001).

100- N. Papanikolaou, Y. Tsougos, and C. Kappas, "The effect of tissue inhomogeneities in IMRT," Proceed. 44th Annual Meeting ASTRO *Med. Phys.* 28(7) (2001).

101- N. Papanikolaou, J. Penagaricano, and V. Ratanatharathorn, "The effect of lung inhomogeneity in IMRT," *Int. J. Radiat. Oncol. Biol. Phys.* 50(Suppl. 1):302 (2001).

102- Epp ER, Lougheed MN, McKay JW. "Ionization build-up in upper respiratory air cavities during teletherapy with cobalt 60 radiation," *Br J Radiol* 31:361–367 (1958).

103- Epp ER, Boyer AL, Doppke KP "Underdosing of lesions resulting from lack of electronic equilibrium in upper respiratory air cavities irradiated by 10-MV x-ray beams," *Int J Radiat Oncol Biol Phys* 2:613– 619 (1977).

104- Niroomand-Rad A, Harter KW, Thobejane S, *et al* "Air cavity effects on the radiation dose to the larynx using Co-60, 6 MV, and 10 MV photon beams," *Int J Radiat Oncol Biol Phys* 29:1139 –1146 (1994).

105- Kan WK, Wu PM, Leung HT, *et al.* "The effect of the nasopharyngeal air cavity on x-ray interface doses," *Phys Med Biol* ;43:529 –537 (1998).

106- Shahine BH, Al-Ghazi MSAL, El-Khatib E. "Experimental evaluation of interface does in the presence of air cavities compared with treatment planning algorithms," *Med Phys* 26:350 –355 (1999).

107- Beach JL, Mendiondo MS, Mendiondo OA. "A comparison of air-cavity inhomogeneity effects for cobalt-60, 6MV and 10-MV x-ray beams," *Med Phys* 14:140 –144 (1987).

108- R. Jeraj and P. Keall, "The effect of statistical uncertainty on inverse treatment planning based on Monte Carlo dose calculat ion," *Phys. Med. Biol.* 45:3601–3613 (2000).

109- R. Jeraj, P. J. Keall, and J. V. Siebers, "The effect of dose calculation accuracy on inverse treatment planning," *Phys. Med. Biol.* 47:391–407 (2002).

110- P. J. Keall, J. V. Siebers, R. Jeraj, and R. Mohan, "The effect of dose calculation uncertainty on the evaluation of radiotherapy plans," Med. Phys. 27:478–84 (2000).

111- I. J. Das, G. X. Ding, and A. Ahnesjö, "Small fields: Nonequilibrium radiation dosimetry," Med. Phys. **35**, 206–215 (2008).

112- M. B. Sharpe, D. A. Jaffray, J. J. Battista, and P. Munro, "Extrafocal radiation: A unified approach to the prediction of beam penumbra and output factors for megavoltage x-ray beams," Med. Phys. **22**, 2065–2074 (1995).

113- T. C. Zhu and B. E. Bjarngard, "The head-scatter factor for small field sizes," Med. Phys. **21**, 65–68 (1994).

114- T. C. Zhu, B. E. Bjarngard, and H. Shackford, "X-ray source and the output factor," Med. Phys. **22**, 793–798 (1995).

115- X. R. Zhu, J. J. Allen, J. Shi, and W. E. Simon, "Total scatter factors and tissue maximum ratios for small radiosurgery fields: Comparison of diode detectors, a parallel-plate ion chamber, and radiographic film," Med. Phys. **27**, 472–477 (2000).

116- T. C. Zhu and K. Manbeck, "CT reconstruction of the x-ray source profile of a medical accelerator," Proc. SPIE **2132**, 242–253 (1994).

117- P. Munro, J. A. Rawlinson, and A. Fenster, "Therapy imaging: Source sizes of radiotherapy beams," Med. Phys. **15**, 517–524 (1988).

118- G. X. Ding, D. M. Duggan, and C. W. Coffey, "Commissioning stereotactic radiosurgery beams using both experimental and theoretical methods,"Phys. Med. Biol. 51, 2549–2566 (2006).

119- A. L. Boyer, T. G. Ochran, C. E. Nyerick, T. J. Waldron, and C. J. Huntzinger, "Clinical dosimetry for implementation of a multileaf collimator," Med. Phys. 19, 1255–1261 (1992).

120- X. A. Li, M. Soubra, J. Szanto, and L. H. Gerig, "Lateral electron equilibrium and electron contamination in measurements of head-scatter factors using miniphantoms and brass caps," Med. Phys. 22, 1167–1170 (1995).

121- IAEA. Report No. 398, "Absorbed Dose Determination in External Beam Radiotherapy: An International Code of Practice for Dosimetry on Standards of Absorbed Dose to Water," Technical Reports Series No. 398, International Atomic Energy Agency, (2000).

122- Task Group-21, Radiation Therapy Committee, AAPM, "A protocol for the determination of absorbed dose from high-energy photon and electron beams," Med. Phys. 10, 741–771 (1983).

123- T. Nyholm, J. Olofsson, A. Ahnesjo, and M. Karlsson, "Modelling lateral beam quality variations in pencil kernel based photon dose calculations," Phys. Med. Biol. 51, 4111–4118 (2006).

124- F. Verhaegen, I. J. Das, and H. Palmans, "Monte Carlo dosimetry study of a 6 MV stereotactic radiosurgery unit," Phys. Med. Biol. **43**, 2755–2768 (1998).

125- F. Sánchez-Doblado, G. H. Hartmann, J. Pena, J. V. Roselló, G. Russiello, and D. M. Gonzalez-Castaño, "A new method for output factor determination in MLC shaped narrow beams," Phys. Medical **23**, 58–66 (2007).

126- A. O. Jones, I. J. Das, and F. L. Jones, "A Monte Carlo study of IMRT46A. O. Jones and I. J. Das, "Comparison of inhomogeneity correction algorithms in small photon fields," *Med. Phys.* **32**, 766–776 (2005).

127- J. Y. Cheung, B. K. Ng, and K. N. Yu, "Dose enhancement close to platinum implants for the 4, 6, and 10 MV stereotactic radiosurgery," *Med. Phys.* **31**, 2787–2791 (2004).

128- H. Saitoh, T. Fujisaki, R. Sakai, and E. Kunieda, "Dose distribution of narrow beam irradiation for small lung tumour," *Int. J. Radiat. Oncol. Biol. Phys.* **53**, 1380–1387 (2002).

129- H. A. Al-Hallaq, C. S. Reft, and J. C. Roeske, "The dosimetric effects of tissue heterogeneities in intensity-modulated radiation therapy (IMRT) of the head and neck," *Phys. Med. Biol.* **51**, 1145–1156 (2006).

130- L. Paelinck, N. Reynaert, H. Thierens, W. De Neve, and C. De Wagter, "Experimental verification of lung dose with radiochromic film: Comparison with Monte Carlo simulations and commercially available treatment planning systems," *Phys. Med. Biol.* **50**, 2055–2069 (2005).

131- T. Krieger and O. A. Sauer, "Monte Carlo- versus pencil-beam /collapsed-cone-dose calculation in a heterogeneous multi-layer phantom,"*Phys. Med. Biol.* **50**, 859–868 (2005).

132- M. M. Aspradakis, R. H. Morrison, N. D. Richmond, and A. Steele, "Experimental verification of convolution/superposition photon dose calculations for radiotherapy treatment planning," Phys. Med. Biol. **48**, 2873–2893 (2003).

133- A. Ahnesjö, "Collapsed cone convolution of radiant energy for photon dose calculation in heterogeneous media," Med. Phys. **16**, 577–592 (1989).

134- I. J. Chetty, P. M. Charland, N. Tyagi, and D. McShan, "Photon beam relative dose validation of the DPM Monte Carlo code in lung-equivalent media," Med. Phys. **30**, 563–573 (2003).

135- Yoon M, Park SY, Shin D, Lee SB, Pyo HR, Kim DY, et al. A new homogeneity index based on statistical analysis of the dose volume Histogram. *J Appl Clin Med Phys.* 8:1–8 (2007).

136- Commissioning User Guide of Eclipse Treatament Planning system for Photon Calculation with Single Pencil Beam Convolution Algorithm *Varian Medical System.* P/N B4 01653R01F; 2:1-92 (2003).

137- Operator's Manual R2.02 of PrecisePLAN® Treatment Planning System Elekta Oncology Systems Ltd., *Manual No. 4513 370 2030 02,* 13:1-20 (2004).

138- Reference Material "External Beam Modeling & Algorithms Prec*ise*PLAN® " Elekta Oncology Systems Ltd., *Manual No. 4513 370 20311,* 3: 1-46 (2003)

139- M. Engelsman, E. M.F. Damen, P. W. Koken, A. A. van 't Veld , K. M. van Ingen, and B. J. Mijnheer, "Impact of simple tissue inhomogeneity correction algorithms on conformal radiotherapy of lung tumours," *Radiother. Oncol.* 60:299–309 (2001).

140- R. Mayer, A. Williams, T. Frankel, Y. Cong, S. Simons, N. Yang, R. Timmerman, "Two-dimensional film dosimetry application in heterogeneous materials exposed to megavoltage photon beams," *Med. Phys.* 24:455–460 (1997).

141- J. E. O'Connor and D. E. Malone, "An equivalent shape approximation for photon doses in lung," *Phys. Med. Biol.* 35(2):223–234 (1990).

142- P. E. Metcalfe, T. P. Wong, and P. W. Hoban, "Radiotherapy x-ray beam inhomogeneity corrections: the problem of lateral electronic disequilibrium in lung," *Australas. Phys. Eng. Sci. Med.* 16:155–167 (1993).

143- P. W. Hoban, D. C. Murray, P. E. Metcalfe, and W. H. Round, "Superposition dose calculation in lung for 10 MV photons," *Australas. Phys. Eng. Sci. Med.* 13:81–92 (1990).

144- T. Knoos, A. Ahnesjo, P. Nilsson, and L. Weber, "Limitations of a pencil beam approach to photon dose calculations in lung tissue," *Phys. Med. Biol.* 40:1411–20 (1995).

145- B. A. Lulu and B. E. Bjarngard, "A derivation of Batho's correction factor for heterogeneities," *Med. Phys.* 9:907–909 (1982).

146- P. J. White, R. D. Zwicker, and D. T. Haung, "Comparison of dose homogeneity effects due to electron equilibrium loss in lung for 6 MV and 18 MV photons," *Int. J. Radiat. Oncol. Biol. Phys.* 34:1141–1146 (1996).

147- E. El-Khatib and J. J. Battista, "Improved lung dose calculation using tissue-maximum ratios in the Batho correction," *Med. Phys.* 11:279–86 (1984).

148- S. J. Thomas, "A modified power-law formula for inhomogeneity corrections in beams of high-energy x-rays," *Med. Phys.* 18:719–23 (1991).